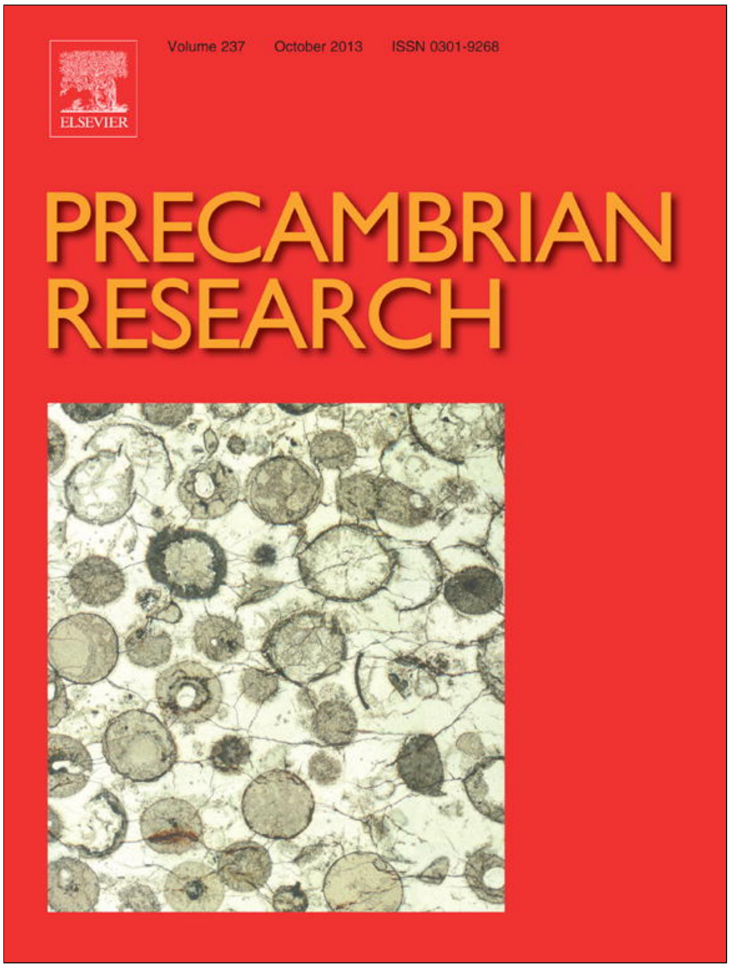
Volume 237 October 2013 ISSN 0301-9268
ELSEVIER
PRECAMBRIAN RESEARCH

Precambrian Research 237 (2013) 13–35

Contents lists available at ScienceDirect

Precambrian Research

journal homepage: www.elsevier.com/locate/precamres

Paleoproterozoic metamorphic and deformation history of the Thompson Nickel Belt, Superior Boundary Zone, Canada, from in situ U–Pb analysis of monazite

Chris G. Couëslan[a,*], David R.M. Pattison[a], S. Andrew Dufrane[b]

[a] Department of Geoscience, University of Calgary, 2500 University Drive NW, Calgary, AB, Canada T2N 1N4
[b] Department of Earth and Atmospheric Sciences, University of Alberta, Edmonton, AB, Canada T6G 2E3

ARTICLE INFO

Article history:
Received 15 September 2012
Received in revised form 10 June 2013
Accepted 24 June 2013
Available online 8 September 2013

Keywords:
Trans-Hudson Orogen
Thompson Nickel Belt
In situ geochronology
Metamorphic monazite
Low-pressure regional metamorphism
Tectonic evolution

ABSTRACT

The Thompson Nickel Belt is a 35 km × 200 km northeast-trending segment of the northwest margin of the Archean Superior craton in Manitoba, bounded to the west by the Paleoproterozoic Reindeer Zone. The belt was metamorphosed and deformed during the Trans-Hudson orogeny, resulting in an elongate, nested metamorphic zonal pattern, parallel to the overall trend of the belt. The metamorphic pattern consists of an inner middle amphibolite-facies zone, flanked on both sides by upper amphibolite-facies zones, flanked in turn by granulite-facies zones. U–Pb data were collected by laser ablation–multiple collector–inductively coupled plasma–mass spectrometry from metamorphic monazite in polished thin sections from each of the metamorphic zones. In the middle amphibolite-facies and upper amphibolite-facies zones, monazite in metapelite is interpreted to have developed during the dominant, foliation-forming deformation event and yields ages of ca. 1776 and 1779 Ma, respectively. Metapelite from the eastern granulite-facies zone contains ca. 1834 Ma monazite grains intergrown with sillimanite that is pseudomorphous after andalusite and grew during the dominant foliation-forming event. Metawacke from the eastern granulite-facies zone contains ca. 1826 Ma and 1792 Ma monazite grains that are interpreted to be contemporaneous with the main foliation-forming event and were unstable in the presence of melt, and a third population of ca. 1748 Ma monazite grains. In the western granulite-facies zone, metapelite contains ca. 1803 Ma monazite grains intergrown with sillimanite that grew during the dominant foliation-forming event, and meta-iron formation contains ca. 1752 Ma monazite grains characterized by oscillatory zoning and associated with melt pseudomorphs. A tectonic model is presented in which the initiation of collision between the Reindeer Zone and the Superior craton begins around ca. 1850–1840 Ma. With continued convergence, rocks now present in the western and eastern granulite-facies zones were progressively buried and heated to middle amphibolite-facies conditions by ca. 1803 and 1792 Ma, respectively. As the collision progressed, rocks now present in the upper amphibolite-facies and middle amphibolite-facies zones were buried and subjected to lower amphibolite-facies metamorphic conditions by ca. 1779 and 1776 Ma, respectively. Progressive regional metamorphism may have been punctuated by local thermal events related to magmatism, such as at ca. 1830 Ma in the eastern granulite-facies zone. Post-peak metamorphic cooling and differential uplift of crustal blocks related to transpressional deformation is recorded by ca. 1752 and 1748 Ma monazite grains from the western and eastern granulite-facies zones, respectively.

1. Introduction

The Thompson Nickel Belt (TNB), part of the Superior Boundary Zone of Manitoba (Bell, 1971; Bleeker, 1990a), occurs on the northwest margin of the Archean Superior craton. This margin was tectonically reworked during the ca. 1.8 Ga Trans-Hudson orogeny in response to convergence with the Archean Hearne craton and intervening Paleoproterozoic rocks of the Reindeer Zone (Fig. 1, Bleeker, 1990a; Ansdell, 2005; Corrigan et al., 2009). The Reindeer Zone consists of oceanic arc-derived rocks that formed in the

* Corresponding author. Present address: Manitoba Geological Survey, Manitoba Innovation, Energy, and Mines, 360-1395 Ellice Avenue, Winnipeg, MB, Canada R3G 3P2. Tel.: +1 204 945 6548; fax: +1 204 945 1406.
E-mail addresses: chris.coueslan@gov.mb.ca, cgcouesl@ucalgary.ca (C.G. Couëslan), pattison@ucalgary.ca (D.R.M. Pattison), dufrane@ualberta.ca (S. Andrew Dufrane).

0301-9268/$ – see front matter © 2013 Elsevier B.V. All rights reserved.
http://dx.doi.org/10.1016/j.precamres.2013.06.009

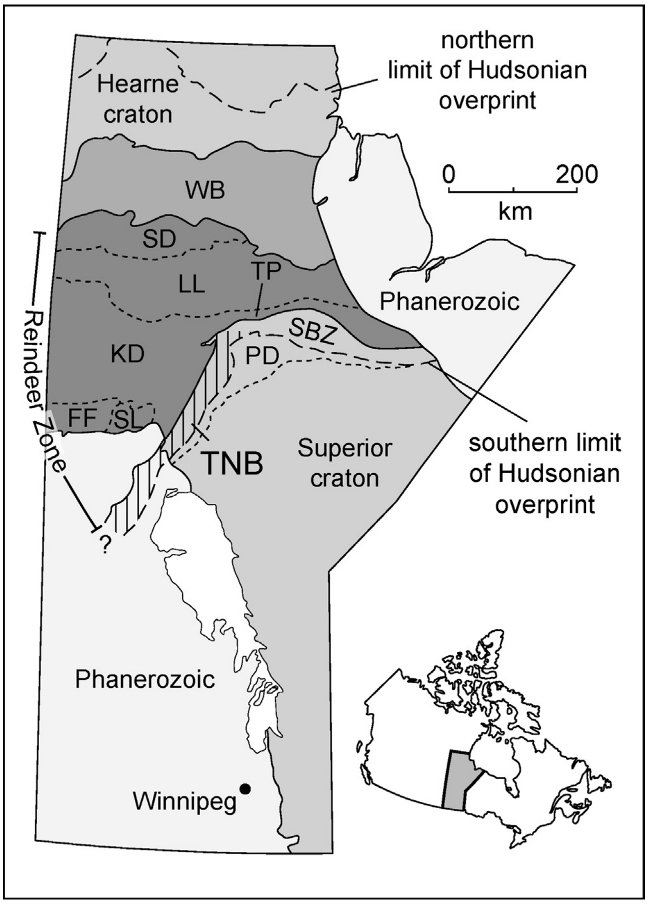

Fig. 1. Simplified tectonic-elements map of Manitoba, Canada (adapted from Lewry et al., 1990; Burnham et al., 2009). Lower right inset shows the location of Manitoba in central Canada. *Abbreviations*: FF, Flin Flon Domain; KD, Kisseynew Domain; LL, Lynn Lake Domain; PD, Pikwitonei Granulite Domain; SBZ, Superior Boundary Zone; SD, Southern Indian Domain; SL, Snow Lake subdomain; TNB, Thompson Nickel Belt; TP, Thompson Promontory; WB, Wathaman Batholith.

Manikewan Ocean (Stauffer, 1984). The exposed northern segment of the TNB, the focus of this study, has a trend of 030°, a width of 30–40 km, and a strike length of approximately 200 km. A southern segment of the belt is covered by Paleozoic limestone and is believed to be continuous over a similar strike length (Burnham et al., 2009).

The majority of geochronological studies in the TNB have utilized grain separates of zircon and monazite to date intrusive rocks. An early period of mafic and felsic magmatism occurred from ca. 1890 to 1870 Ma, and was followed by relatively continuous, dominantly felsic magmatism from ca. 1853 to 1770 Ma with granitic pegmatite dykes reported as young as 1727 Ma (Machado et al., 1990, 2011a,b; Bleeker et al., 1995; Bleeker and Macek, 1996; Zwanzig et al., 2003; Percival et al., 2004, 2005; Machado et al., 2011a,b). Grain separates of zircon and monazite from metamorphic rocks have yielded ages between ca. 1810 and 1750 Ma, broadly interpreted to represent the timing of peak metamorphism in the belt (Machado et al., 1990, 2011a; Rayner et al., 2006; Schneider et al., 2007; Burnham et al., 2009; Heaman et al., 2009). Grain separates of titanite from metamorphic rocks yielded ages ranging from ca. 1799 to 1720 Ma (Bleeker et al., 1995; Zwanzig et al., 2003; Scoates et al., 2010; Machado et al., 2011a), and have been variously interpreted to date peak and retrograde metamorphic events. A thermochronology study by Schneider et al. (2007) obtained $^{40}Ar/^{39}Ar$ ages for hornblende and biotite separates which ranged from ca. 1745 to 1723 Ma and 1789 to 1701 Ma, respectively.

Although there appears to be an abundance of geochronological data, the timing of many of the tectonometamorphic events that affected the TNB remains poorly constrained. The major phase of regional penetrative deformation, D_2, is reported to be as young as ca. 1820 to 1770 Ma (Bleeker, 1990b); however, Machado et al. (2011a) interpreted D_2 as occurring between ca. 1890 and 1885 Ma. Interpretations for the timing of peak metamorphic conditions in the belt range from ca. 1820 Ma (White et al., 1999) to ca. 1770 Ma (Rayner et al., 2006). A later regional deformation event, D_3, accompanied by retrograde metamorphism, is interpreted to have occurred as early as ca. 1850–1750 Ma (Machado et al., 2011a) and as late as ca. 1770–1700 Ma (Bleeker, 1990b). Complications to the above interpretation include: the presence of metamorphic zircon as young as ca. 1750 Ma, interpreted to date peak metamorphism (Burnham et al., 2009), and $^{40}Ar/^{39}Ar$ ages of biotite as old as ca. 1789 Ma (Schneider et al., 2007).

This study uses in situ U–Pb dating of metamorphic monazite by laser ablation–multiple collector–inductively coupled plasma–mass spectrometry (LA–MC–ICP–MS) to help clarify some of these issues. In situ dating of monazite allows for direct linking of age information to deformational fabrics and metamorphic assemblages, and allows for the dating of discrete zones within grains (Williams and Jercinovic, 2002; Simonetti et al., 2006). The new data are used to refine our understanding of the metamorphic and deformational history of the TNB.

2. Regional geology

2.1. The Kisseynew Domain

Before discussing the geology of the TNB, it is necessary to briefly describe the geology of the adjacent Kisseynew Domain because of its involvement with the tectonic evolution of the TNB. The Kisseynew Domain occurs immediately to the west of the TNB, and is part of the Reindeer Zone. It represents either a back-arc or fore-arc basin comprising predominantly turbidite-derived metagreywacke of the Burntwood Group, the latter deposited from ca. 1855 to 1840 Ma (Percival et al., 2005; Zwanzig et al., 2007; Zwanzig and Bailes, 2010). Detrital zircon grains yield ages of ca. 1930–1840 Ma, suggesting derivation from the surrounding juvenile magmatic arcs (Percival et al., 2005). The Grass River Group (Zwanzig et al., 2007) is a subaerial to shallow-water clastic sequence of metaconglomerate to arkosic metasandstone that was deposited along the west flank of the TNB. The Grass River Group is believed to be the shallow-water equivalent to the Burntwood Group and was deposited contemporaneously with similar arkosic sequences along the southern and northern flanks of the Kisseynew Domain (Missi and Sickle groups, respectively, Zwanzig et al., 2007). The presence of the largely arc-derived Grass River Group along the west flank of the TNB suggests early (minimum, ca. 1840 Ma) interaction of that belt with the Reindeer Zone.

The boundary between the Kisseynew Domain and the TNB was historically considered to be a major terrane bounding fault (Bell, 1971; Bleeker, 1990a); however, the boundary between the Kisseynew Domain and the TNB is no longer simply defined (Fig. 2). Structural domes up to 60 km west of the TNB, in the eastern Kisseynew Domain, are cored by Archean gneisses and an Ospwagan Group-like cover sequence with zircon populations typical of the Superior craton (Percival et al., 2006; Zwanzig et al., 2006). Interleaving of Ospwagan Group and Burntwood Group rocks in the northern part of the TNB suggests early thrusting of the Kisseynew Domain onto the TNB along a low angle fault prior

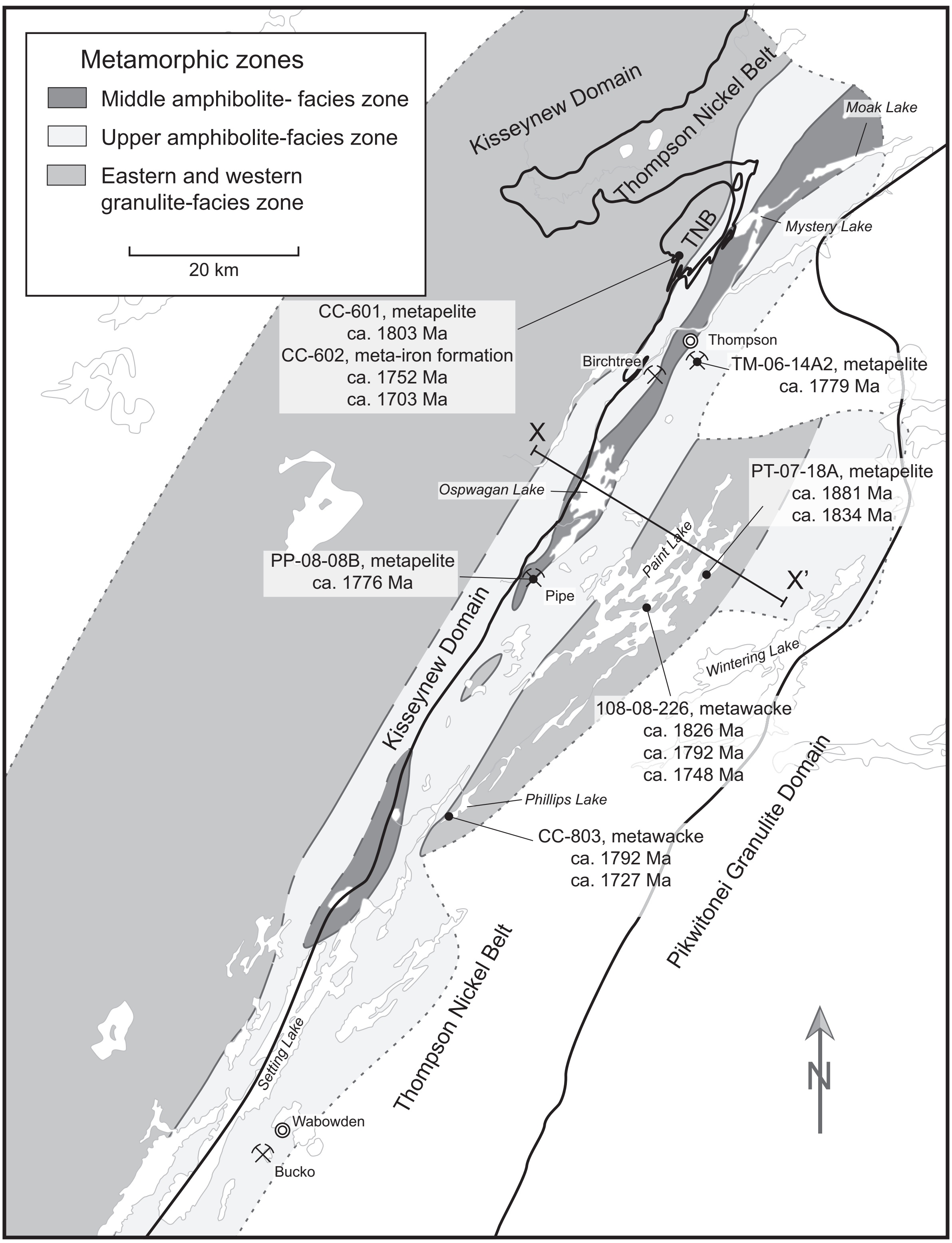

Fig. 2. Metamorphic-facies map of the exposed segment of the TNB and adjacent Kisseynew Domain (modified from Couëslan and Pattison, 2012). Heavy black lines indicate the approximate boundaries of the TNB with the Kisseynew Domain to the west and the Pikwitonei Granulite Domain to the east. Solid gray lines define facies-zone boundaries, dashed lines define inferred boundaries, and dotted lines define the limits of data. Line X–X′ indicates the approximate position of the schematic cross-section in Fig. 12f. Sampling locations along with the weighted mean $^{207}Pb/^{206}Pb$ ages are indicated by black dots. *Abbreviations*: TNB, Thompson Nickel Belt rocks.

to nappe development (Zwanzig and Böhm, 2002; Percival et al., 2006; Zwanzig et al., 2006). The TNB and adjacent parts of the Kisseynew Domain therefore likely had a shared tectonic history starting with D_2 (see Section 2.3).

2.2. Thompson Nickel Belt

The TNB largely consists of reworked Archean gneiss of the Superior craton. The gneiss is interpreted to be derived from the adjacent Pikwitonei Granulite Domain which was subjected to amphibolite- to granulite-facies conditions from ca. 2720 to 2640 Ma (Fig. 2, Hubregtse, 1980; Mezger et al., 1990; Heaman et al., 2011). The Pikwitonei granulites were exhumed and unconformably overlain by the Paleoproterozoic supracrustal rocks of the Ospwagan Group (Scoates et al., 1977; Bleeker, 1990a; Zwanzig et al., 2007). The Ospwagan Group metasedimentary sequence consists of a fining upward siliciclastic sequence (Manasan Formation), grading into calcareous metasedimentary rocks of the Thompson Formation. The Thompson Formation is overlain by deeper basin siliciclastic and chemical metasedimentary rocks of the Pipe Formation, which grade into the Setting Formation, a coarsening upward siliciclastic package. The Setting Formation is capped by a thick sequence of mafic to ultramafic metavolcanic rocks of the Bah Lake Assemblage (Bleeker, 1990a; Zwanzig et al., 2007). Paleoproterozoic detrital zircons have been extracted from the Manasan and Setting formations, yielding maximum ages for deposition of ca. 2.24 Ga and 1.97 Ga, respectively (Bleeker and Hamilton, 2001; Machado et al., 2011a). A minimum age for the Ospwagan Group is provided by cross-cutting amphibolitized dykes interpreted to be part of the ca. 1880 Ma Molson dyke swarm, and the possibly co-magmatic nickel ore-bearing ultramafic sills, which intruded the Ospwagan Group supracrustals at all stratigraphic levels at ca. 1880 Ma (Bleeker, 1990a; Heaman et al., 2009; Scoates et al., 2010).

2.3. Deformation

The Ospwagan Group was affected by four main generations of deformation during the Trans-Hudson orogeny (Bleeker, 1990a; Burnham et al., 2009). Early deformation (D_1) pre-dates the ca. 1880 Ma mafic magmatism (Molson dykes); however, this early deformation is largely obscured by later deformation. F_1 folds are only observed where suitable markers such as cross-cutting mafic dykes are present. Although Bleeker (1990a) interpreted this deformation phase as the main nappe-forming event, it is now recognized that Kisseynew Domain rocks belonging to the Burntwood and Grass River groups are infolded into the western-most nappe structures, and that these supracrustal groups post-date the ca. 1880 Ma magmatic event (ca. 1855–1840 Ma, Percival et al., 2005; Zwanzig et al., 2007). The D_1 deformation phase is now tentatively interpreted as a relatively upright folding event (Burnham et al., 2009).

The dominant phase of penetrative deformation is D_2. Molson dykes are deformed by D_2 and typically display an S_2 foliation. The F_2 fold generation refolded and tightened F_1 folds in metasedimentary lithologies and resulted in isoclinal to recumbent F_2 folds which also incorporated the underlying Archean gneiss. The recumbent folds have been interpreted as either east-verging (Bleeker, 1990a; White et al., 2002), or southwest-verging (Zwanzig et al., 2006; Burnham et al., 2009). The recumbent folds are accompanied by regionally penetrative S_2 fabrics. Microstructural observations (Couëslan and Pattison, 2012) suggest that peak metamorphic conditions were attained during, and possibly outlasted D_2. The D_3 generation of deformation resulted in tight, vertical to steeply southeast-dipping, isoclinal F_3 folds (Bleeker, 1990a; Burnham et al., 2009). The isoclinal nature of both F_2 and F_3 results in a co-planar relationship between S_2 and S_3 along F_3 fold limbs. Mylonite zones with subvertical stretching lineations parallel many of the regional F_3 folds, and are characterized by retrograde lower amphibolite- to greenschist-facies mineral assemblages (Bleeker, 1990a; Burnham et al., 2009). Tightening of F_2–F_3 structures continued during D_4, marked by localized retrograde greenschist metamorphism along mylonitic and brittle cataclastic, northeast-striking shear zones that commonly indicate southeast-side-up, sinistral movement (Bleeker, 1990a; Burnham et al., 2009). The D_3–D_4 structures appear to exert a first order control on the present day distribution of metamorphic zones within the belt (Couëslan and Pattison, 2012).

2.4. Metamorphism

The TNB can be divided into three regional, nested metamorphic zones – middle amphibolite-facies, upper amphibolite-facies, and granulite-facies – which subparallel the strike of the belt and the regional D_3–D_4 structures (Fig. 2, Couëslan and Pattison, 2012). Peak metamorphism and associated isograds were established prior to D_3, and the metamorphic-facies isograds were then deformed by D_3–D_4 structures into their current configuration (Couëslan and Pattison, 2012).

Middle amphibolite-facies rocks occur in two elongate domains along the axis of the belt: a southerly domain at the north end of Setting Lake that straddles the boundary with the Kisseynew Domain, and a more northerly domain stretching from Pipe mine in the south, through the city of Thompson, to north of Mystery and Moak lakes (Fig. 2). In this zone, metapelitic schist contains quartz + plagioclase + muscovite + biotite plus combinations of garnet, sillimanite, andalusite, and staurolite. Hornblende + plagioclase-bearing metabasite contain combinations of biotite, cummingtonite, quartz and clinopyroxene. Quartz + grunerite + hornblende + biotite + pyrrhotite + magnetite-bearing meta-iron formation is commonly garnet-bearing. Metamorphic conditions in the middle amphibolite-facies zone are estimated to be 550–620 °C and 300–500 MPa, with the pressure increasing from Pipe mine toward the north (Couëslan and Pattison, 2012).

The middle amphibolite-facies domains are flanked to the southeast and northwest by upper amphibolite-facies zones, which join south of Pipe mine (Fig. 2). In this zone, metapelitic gneiss is typically migmatitic and contains quartz + plagioclase + K-feldspar + biotite + sillimanite ± garnet. Meta-iron formation contains quartz + orthopyroxene + biotite + hornblende + pyrrhotite + magnetite and combinations of garnet and K-feldspar. Metabasic gneiss contains the same mineral assemblages observed at middle amphibolite-facies conditions. The metamorphic conditions in the upper amphibolite-facies zone are estimated to be 640–755 °C and 300–600 MPa, with pressures increasing from Pipe mine toward the north (Couëslan and Pattison, 2012).

Flanking the upper amphibolite-facies zones are granulite-facies zones: an eastern granulite-facies zone centered around Paint Lake, and a western granulite-facies zone that encompasses the northwest portion of the TNB and continues west to include much of the adjacent Kisseynew Domain (Fig. 2). In this zone, migmatitic metapelitic gneiss contains quartz + K-feldspar + plagioclase + biotite + cordierite + garnet + sillimanite ± spinel. Metabasic gneiss contains hornblende + plagioclase + orthopyroxene + clinopyroxene and combinations of garnet, biotite, and quartz. Meta-iron formation contains quartz + orthopyroxene + biotite + garnet + K-feldspar + pyrrhotite and combinations of magnetite and plagioclase. Metamorphic conditions in the granulite-facies zone are estimated at 775–830 °C and 500–700 MPa (Couëslan and Pattison, 2012).

3. Analytical methods

Monazite was identified using element-distribution maps of carbon-coated thin sections for Ce, Ca, Al, Si, and P by wavelength dispersive spectrometry (WDS) using a JEOL JXA-8200 Superprobe at the University of Calgary Laboratory for Electron Microbeam Analysis (UCLEMA). The element maps were generated using a method similar to Williams and Jercinovic (2002) with a 15 kV accelerating voltage, 50 nA beam current, defocused beam (35 μm), 35 μm step size, and a dwell time of 10 ms over a 950 × 500 point grid. The element maps were used for the identification of monazite and placing the grains into textural context. Back-scattered electron (BSE) images were taken of all monazite grains analyzed for this study. Element-distribution maps of selected monazite grains were made for Ce, U, Th, Pb, and Y, using WDS with an accelerating voltage of 15 kV, beam current of 60 nA, focused beam, and a dwell time of 40 ms over an 800 × 800 point grid. The element maps were compared with BSE images of the grains and brighter zones were found to correlate with elevated Th and Pb, while darker zones correlated with elevated Y.

Uranium and Pb isotopic data was acquired at the Radiogenic Isotope Facility at the University of Alberta using a Nu Plasma multiple collector–inductively coupled plasma–mass spectrometer coupled to a New Wave Research UP213 laser ablation system. Both the instrument parameters and measurement protocols are outlined in Simonetti et al. (2005, 2006). Corrections for laser induced element fractionation and instrument drift/bias were achieved by analysis of an external monazite standard (Western Australia, 2842.9 ± 0.3 Ma, Simonetti et al., 2006) after the analysis of every 10–12 unknowns. A beam diameter of 12 μm was used for all samples except for sample PT-07-18A, in which the monazite grains are characterized by higher concentrations of U and Pb which necessitated using a beam diameter of 8 μm to reduce the strength of the ion signal being sent to the ion counters. The U–Pb data can be found in Appendix A. Reflected light photomicrographs were taken before and after analyses of the monazite grains so that ablation pits could be accurately placed on BSE images. All U–Pb isotopic plots were constructed with Isoplot version 3.0 (Ludwig, 2003). Errors are reported at the 2σ confidence level and are a quadratic combination of the standard internal measurement error and the external reproducibility of the monazite standard. Typical reproducibility is 1% for $^{207}Pb/^{206}Pb$ and 3% for $^{206}Pb/^{238}U$, though in some of the analyses here, the reproducibility is much higher, particularly for $^{206}Pb/^{238}U$.

4. U–Pb results

The locations of samples are shown in Fig. 2. One sample comes from the middle amphibolite-facies zone, one sample comes from the upper amphibolite-facies zone, and five samples come from the granulite-facies zone. Of the latter, three come from the eastern granulite-facies zone and two come from the western granulite-facies zone. Mineral abbreviations used in the text and figures are from Kretz (1983).

4.1. Middle amphibolite-facies

A sample of Pipe Formation metapelite (PP-08-08B) was collected at the Pipe II mine (Fig. 2). The sample is a fine-grained schist containing the assemblage Qtz + Bt + Ms + Pl + St + And + Sil + Grt (Couëslan et al., 2011; Couëslan and Pattison, 2012). Porphyroblasts of garnet, andalusite, and staurolite are wrapped by the S_2 foliation. Fibrous sillimanite aligned along S_2 is common. Monazite grains are typically hosted in the matrix and occur in both quartzofeldspathic and micaceous layers. One monazite grain was noted as an inclusion in a garnet porphyroblast (Fig. 3 a). Monazite grains are granoblastic and subequant with local quartz inclusions. Patchy or domainal zoning is commonly observed in BSE images of monazite, with margins between domains ranging from sharp to diffuse (Fig. 3b). The fine-scale zoning occurs on a scale that is below the resolution of the 12 μm beam size of the laser.

Five monazite grains from this sample were of sufficient size for analysis. The monazite grains are small (typically <50 μm in the longest dimension). As a result, only one to two spots were analyzed per grain. The results plot near concordia (Fig. 4a) and within error of each other, suggesting the monazite grains represent either a single generation, or formed over a period of time that is within the uncertainty of the analytical technique. The calculated $^{207}Pb/^{206}Pb$ ages of the analyses range from ca. 1785 to 1769 Ma (Appendix A). There is a sufficient spread of the data to define a discordia with an upper intercept of 1773 + 20/−16 Ma. The weighted mean $^{207}Pb/^{206}Pb$ age of 1776 ± 7 Ma is identical within error.

4.2. Upper amphibolite-facies

A sample of Pipe Formation metapelite (TM-06-14A2) was collected from the Thompson mine (Fig. 2). The metapelite is medium grained and migmatitic, and contains the mineral assemblage Bt + Qtz + Pl + Sil + Kfs + Grt (Couëslan and Pattison, 2012). The leucosome forms discontinuous veinlets parallel to S_2. Fibrous to fine-grained acicular sillimanite is typically intergrown with biotite, and locally forms discontinuous laminae, and discrete flattened knots, all parallel to S_2. Garnet porphyroblasts are wrapped by S_2. Monazite most commonly occurs in the matrix but rarely occurs as inclusions in garnet. It is generally granoblastic and subequant, but is locally elongate, and may display finger-like protuberances, parallel to S_2 (Fig. 3c). Concentric and patchy zoning is common in BSE images of monazite, but the zoning usually occurs at a resolution smaller than the diameter of the laser beam (Fig. 3c). Fine-grained quartz inclusions are locally present in the monazite grains.

Analyses from seven monazite grains were used for age determination calculations. One to four analyses were made of each monazite depending on the size of the grain. The results plot near concordia, and within error of each other suggesting a single age population (Fig. 4b). The grains yielded $^{207}Pb/^{206}Pb$ ages ranging from ca. 1808 to 1763 Ma (Appendix A), and a weighted mean $^{207}Pb/^{206}Pb$ age of 1779 ± 5 Ma.

4.3. Granulite-facies

Three samples were analyzed from the eastern granulite-facies zone: a ferruginous metawacke was collected from diamond drill core from Phillips Lake (CC-803), and samples of metapelite (PT-07-18A) and ferruginous metawacke (108-08-226) were collected from Paint Lake (Fig. 2). All samples are from a metasedimentary sequence of uncertain affinity that consists of interbedded ferruginous metawacke and metapsammite with minor metapelite and silicate-facies iron formation. The sequence does not correspond to any of the Paleoproterozoic supracrustal groups previously recognized in the region; however, it has been tentatively interpreted as Paleoproterozoic by Couëslan (2012) based on a limited dataset of detrital zircon analyses that included an age mode at ca. 2440 Ma. A further two samples were analyzed from the western granulite-facies zone, a sample of metapelitic gneiss (CC-601) and a sample of meta-iron formation (CC-602) from the Pipe Formation of the Ospwagan Group. Both samples were collected from a single diamond drillhole located 9.5 km north of the city of Thompson (Fig. 2).

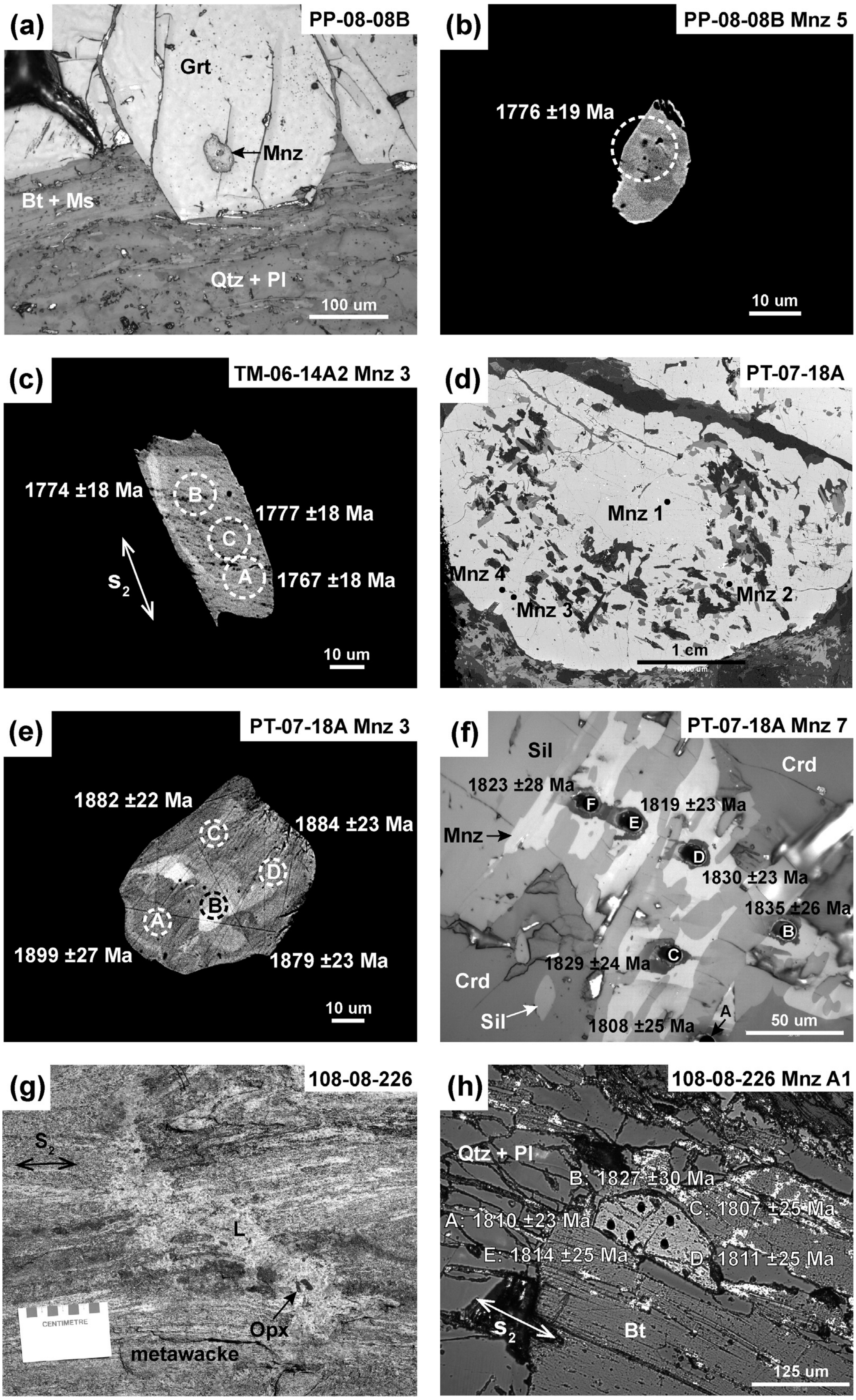

Fig. 3. (a) Photomicrograph in reflected light of monazite included in garnet, metapelite sample PP-08-08B, middle amphibolite-facies zone. The garnet porphyroblasts are weakly wrapped by the S_2 foliation; (b) back-scattered electron image of monazite 5, metapelite sample PP-08-08B. The dashed circle indicates the location of the ablation pit along with the calculated $^{207}Pb/^{206}Pb$ age; (c) back-scattered electron image of monazite 3, metapelite sample TM-06-14A2, upper amphibolite-facies zone. Minor growth along the left side of the grain is parallel to adjacent grains of S_2 biotite; (d) back-scattered electron image of a coarse-grained garnet from metapelite sample PT-07-18A, eastern granulite-facies zone. The garnet consists of an inclusion-poor core, inclusion-rich annulus, and inclusion-poor rim. The locations of analyzed monazite grains are

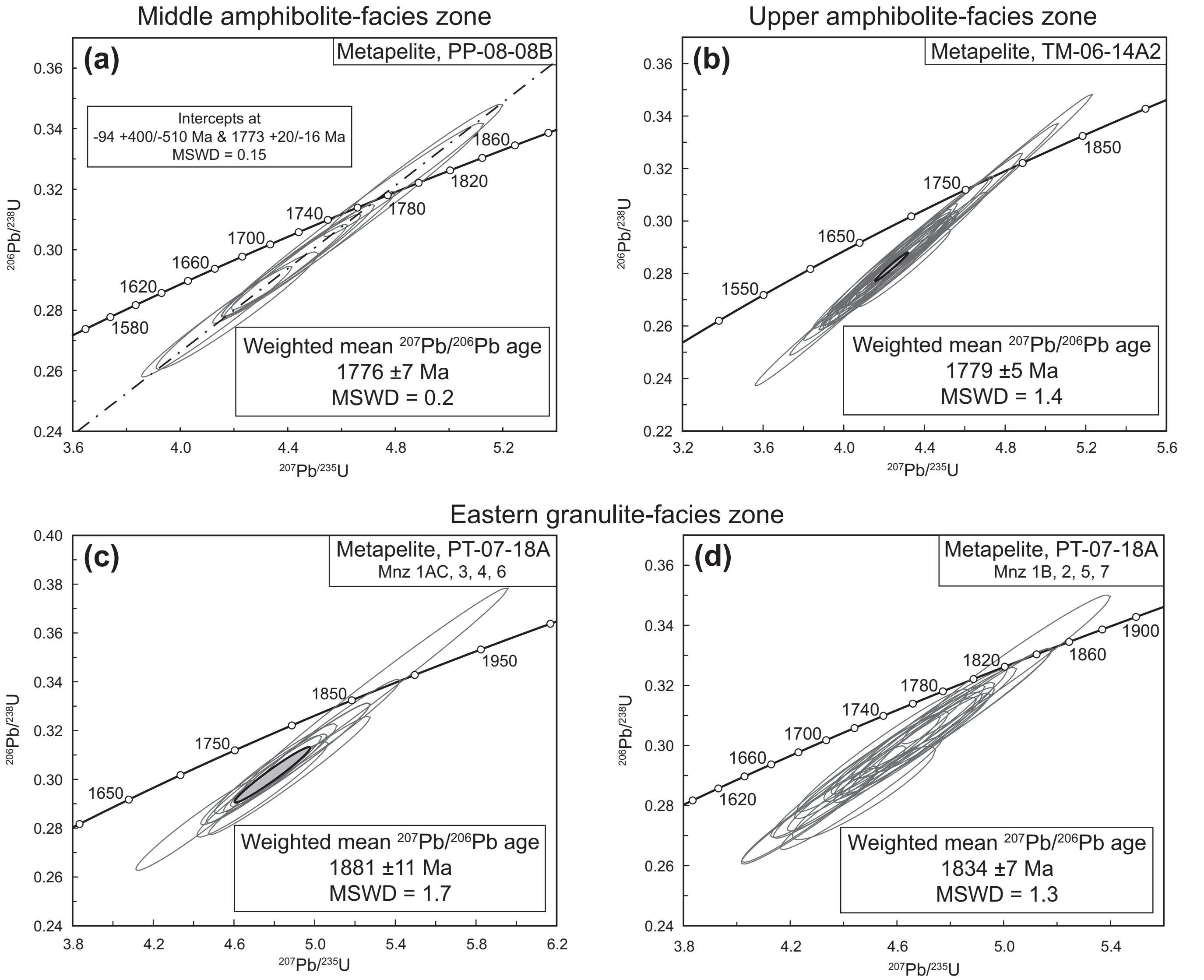

Fig. 4. U–Pb laser ablation results of monazite from metapelite samples (a) PP-08-08B, Pipe II mine, middle amphibolite-facies zone; (b) TM-06-14A2, Thompson mine, upper amphibolite-facies zone; and (c) and (d) PT-07-18A, Paint Lake, eastern granulite-facies zone. See text for details.

4.3.1. Eastern granulite facies, PT-07-18A, metapelite

The metapelite sample was collected from an island near the eastern shore of Paint Lake (Fig. 2). Discontinuous bands and boudins of amphibolite are also present within the outcrop, which are interpreted as metadiabase dykes. The metapelite is migmatitic, coarse grained, and contains the assemblage Bt + Qtz + Crd + Pl + Grt + Sil + Kfs (Couëslan and Pattison, 2012). Discontinuous veins of leucosome are sheared and oriented subparallel to S_2. The melanosome consists mostly of biotite, cordierite, garnet, and sillimanite. The sillimanite occurs as monocrystalline and polycrystalline pseudomorphs after andalusite and as fine-grained inclusions in cordierite, parallel to S_2 (Couëslan and Pattison, 2012). The pseudomorphous sillimanite is enclosed, and partially replaced, by granoblastic cordierite. Coarse-grained (2–4 cm) garnet porphyroblasts are commonly enveloped by leucosome. The garnet is characterized by an inclusion-rich annulus (Fig. 3d) containing sillimanite, staurolite, and spinel–sillimanite intergrowth replacing staurolite. Both the garnet and pseudomorphed andalusite are wrapped by S_2.

Seven grains of monazite were analyzed with one to seven spots per grain. Monazite grains 1–4 are inclusions in a large (4 cm) porphyroblast of garnet (Fig. 3d). Monazite 1, 3, and 4 are subequant and characterized by sharp, complex domainal zoning in BSE images (Fig. 3e). Monazite 2 is from the inclusion-rich annulus of the garnet; it is a tabular and relatively homogeneous grain with wispy, diffuse zoning present in BSE images. Monazite grains 5 and 7 occur as fine-grained intergrowths with sillimanite (Fig. 3f) that is pseudomorphous after andalusite (Couëslan and Pattison, 2012). Back-scattered electron images of monazite 5 and 7 show the grains to be relatively homogeneous. Monazite 6 is a subequant grain enclosed by biotite and has complex zoning similar to monazite 1, 3, and 4.

marked by black dots; (e) back-scattered electron image of monazite 3, sample PT-07-18A. The grain displays complex, patchy zoning; (f) photomicrograph in reflected light of monazite 7, sample PT-07-18A. The monazite is intergrown with sillimanite that is pseudomorphous after andalusite; (g) outcrop photograph of sampling location 108-08-226 showing locally derived leucosome cross-cutting the S_2 fabric. Scale card is in cm; and (h) photomicrograph in reflected light of monazite A1, sample 108-08-226. The monazite is located in the matrix of the metawacke and is elongate parallel to the S_2 fabric. *Abbreviations*: L, leucosome. Mineral abbreviations are from Kretz (1983).

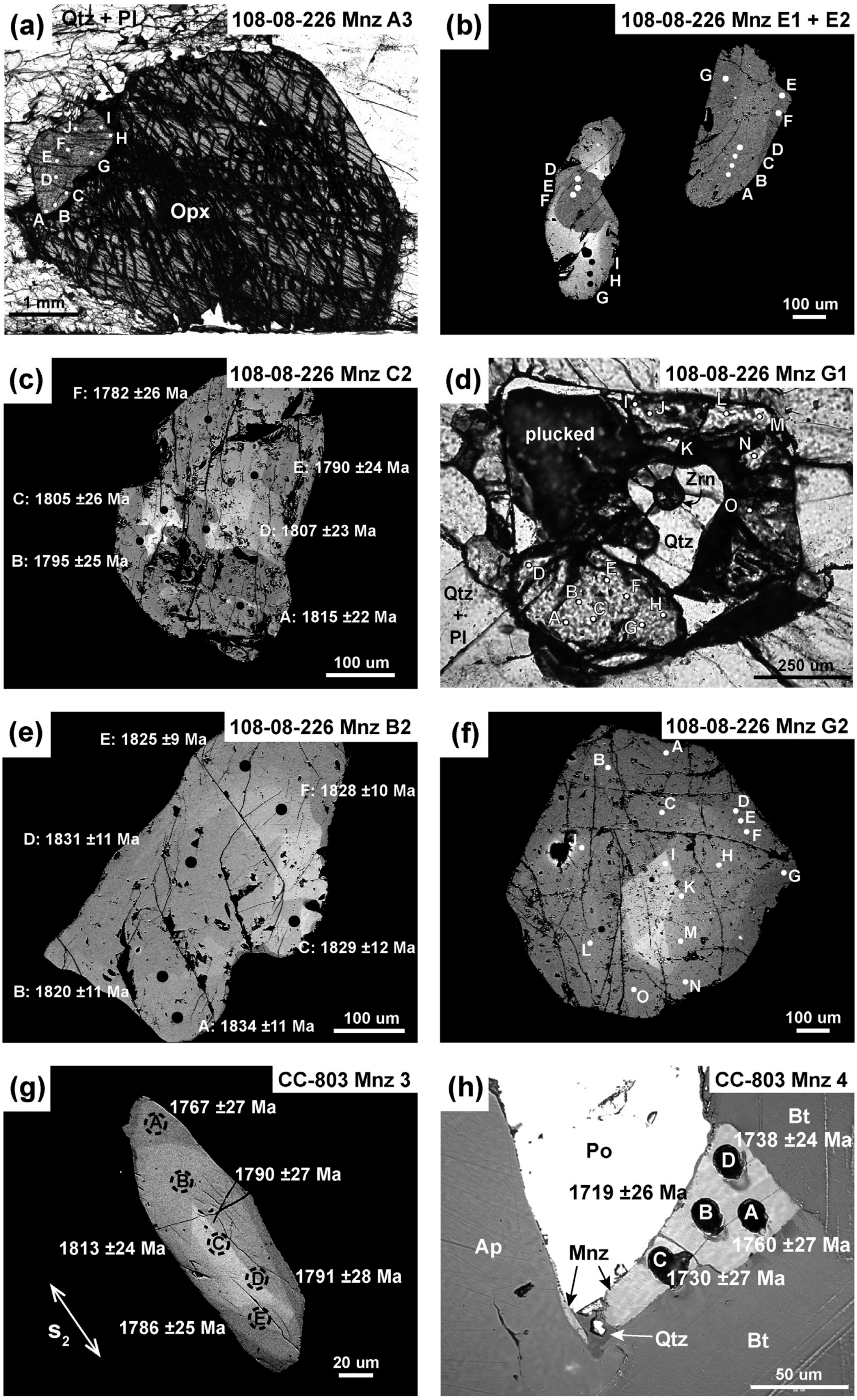

Fig. 5. (a) Photomicrograph in transmitted light of monazite A3, sample 108-08-226. The monazite is partially enclosed by a porphyroblast of orthopyroxene within the leucosome matrix. The white markers used to indicate the locations of ablation pits are not to scale; (b) back-scattered electron image of monazite E1 (left) and E2 (right), sample 108-08-226. Monazite E1 is characterized by both sharp and diffuse zoning; (c) back-scattered electron image of monazite C2, sample 108-08-226. The monazite is rounded and characterized by complex patchy zoning; (d) photomicrograph in transmitted light of monazite G1, sample 108-08-226. The monazite is embayed and in-filled by quartz. The upper left-hand portion of the grain was plucked during polishing; (e) back-scattered electron image of monazite B2, sample 108-08-226. Roughly concentric zoning

The calculated $^{207}Pb/^{206}Pb$ ages of the analyses range from ca. 1914 to 1808 Ma (Appendix A). The distribution of $^{207}Pb/^{206}Pb$ ages suggests at least two distinct periods of monazite growth. The subequant, complexly zoned monazite included in garnet and enclosed by biotite form an older age group (monazite 1, 3, 4, and 6, typically >ca. 1870 Ma), whereas the less complexly zoned monazite included in garnet and the monazite intergrown with sillimanite form a younger age group (monazite 2, 5, and 7, typically <1845 Ma). An analysis from the rim of monazite 1 also falls into the younger age group. The complexly zoned monazite yield slightly discordant data and appear to define a single population (Fig. 4c). The weighted mean $^{207}Pb/^{206}Pb$ for the complexly zoned monazite is 1881 ± 11 Ma. The monazite of the younger age group appear to define a second slightly discordant population (Fig. 4d), and yield a weighted mean $^{207}Pb/^{206}Pb$ age of 1834 ± 7 Ma.

4.3.2. Eastern granulite facies, 108-08-226, ferruginous metawacke

The metawacke was collected from an island in central Paint Lake (Fig. 2). The outcrop consists of layered metawacke with local segregations of unfoliated leucosome that cross-cut the S_2 foliation and appears to be locally derived/in-situ (Fig. 3g). The metawacke contains the assemblage Pl + Qtz + Bt + Opx + Kfs + Grt (Couëslan and Pattison, 2012). Orthopyroxene in the melanosome is typically elongate parallel to S_2. Patches of leucosome are typically massive with randomly oriented porphyroblasts of orthopyroxene in a medium to coarse-grained, quartzofeldspathic matrix. Seven samples were collected at the relatively diffuse contacts between the metawacke and leucosome.

Eighteen monazite grains were analyzed with four to 15 analyses per grain. Monazite A1 and A2 occur within the matrix of the metawacke. Monazite A1 is sub-idiomorphic and elongate parallel to S_2 (Fig. 3h), while monazite A2 is subequant and xenomorphic. Both grains are characterized by diffuse patchy zoning. Monazite A3 and E1 occur within the matrix of leucosome and are partially overgrown by porphyroblasts of orthopyroxene (Fig. 5a). Monazite A3 is subequant with minor embayments and characterized by diffuse, broadly concentric zoning. Monazite E1 is elongate with rounded terminations and characterized by sharp to diffuse patchy zoning (Fig. 5b). Monazite B1, C1, C2, D2, E2, E3, E4, and G1 occur within the matrix of leucosome. Grains B1, C1, C2, and E4 are subequant and locally embayed, and characterized by patchy zoning (Fig. 5c). Monazite D2 and E2 are sub-idioblastic, and relatively homogeneous (Fig. 5b). Monazite E3 is idioblastic and shares triple point grain boundaries with surrounding grains of plagioclase and quartz. It is characterized by diffuse concentric and patchy zoning. Monazite G1 appears sub-idioblastic with rounded corners and an embayment that penetrates to the core of the grain (Fig. 5d). The embayment is filled in with quartz and contains a rounded, presumably detrital grain of zircon. Monazite G1 appears relatively homogeneous in BSE images. Monazite B2, F1, F2, F3, and F4 occur entrained within schlieric material at the boundary between metawacke and leucosome. Grain B2 appears embayed, is slightly elongate parallel to S_2, and is characterized by roughly concentric zoning that is truncated by the grain margin (Fig. 5e). Monazite F1, F2, F3, and F4 are subequant and granoblastic with relatively subdued, patchy zoning. Monazite G2 occurs as an inclusion in a coarse-grained, perthitic K-feldspar porphyroblast in leucosome. It is equant and sub-idioblastic and characterized by concentric zoning (Fig. 5f).

The calculated $^{207}Pb/^{206}Pb$ ages of the analyses range from ca. 1834 to 1720 Ma (Appendix A). The distribution of $^{207}Pb/^{206}Pb$ ages suggests at least three periods of monazite growth. Monazite B1 and B2 are both characterized by complex patchy zoning and embayed grain boundaries, and define the oldest age group (typically >ca. 1825 Ma). Monazite F1, F2, F3, and F4 are all granoblastic grains with subdued zoning that occur within schlieric material. These four grains define the youngest age population with $^{207}Pb/^{206}Pb$ ages typically <ca. 1755 Ma. The remaining monazite analyses define the middle and largest age population (typically ca. 1810–1770 Ma). Monazite from this middle population include grains from the metawacke matrix that are elongate parallel to S_2 (monazite A1), grains from the leucosome matrix that are partially overgrown by orthopyroxene porphyroblasts (monazite A3 and E1), grains from the leucosome matrix that appear embayed (monazite A3, B1, E4, G1), and a single grain that was included in a K-feldspar porphyroblast in the leucosome (monazite G2). The oldest and middle age populations both yield slightly discordant data and weighted mean $^{207}Pb/^{206}Pb$ ages of 1826 ± 4 Ma and 1792 ± 3 Ma, respectively (Fig. 6a and b). The spread of data for the youngest age population defines a discordia with an upper intercept of 1745 + 6/−9 Ma which is identical within error to the weighted mean $^{207}Pb/^{206}Pb$ age of 1748 ± 4 Ma (Fig. 6c).

4.3.3. Eastern granulite facies, CC-803, ferruginous metawacke

The ferruginous metawacke is medium grained, migmatitic, and contains Pl + Qtz + Bt + Opx + Grt + Kfs. Biotite defines the main fabric of the rock (S_2); however, local strong alignment along discrete folia may represent S_3. Thin discontinuous veinlets containing quartz and antiperthite are ubiquitous and are oriented parallel to S_2 and are interpreted as crystallized veinlets of melt. Orthopyroxene is commonly elongate parallel to S_2. Porphyroblasts of garnet are typically xenomorphic.

Monazite grains vary from subequant and granoblastic to tabular and idioblastic, and are characterized by well defined concentric zoning in BSE images. Zoning consists of bright cores with elevated Th enclosed by two to three zones that become progressively darker, and enriched in Y, toward the rim (Fig. 5g). Tabular grains are commonly elongate parallel to S_2. Monazite 4 is unique in that it is characterized by more diffuse zoning and at one end the grain is intergrown with quartz and forms a thin film along an apatite grain boundary (Fig. 5h).

Four grains of matrix-hosted monazite were analyzed with two to five analyses per grain. The analyses yielded $^{207}Pb/^{206}Pb$ ages ranging from ca. 1813 to 1719 Ma (Appendix A), which appear to define two distinct age groups. Although the concentric zoning in the idioblastic grains (monazite 2 and 3) appear to display a general trend of older $^{207}Pb/^{206}Pb$ ages in the cores and younger ages in the rims (Fig. 5g), the ages are within error of one another and define the oldest age group with a weighted mean $^{207}Pb/^{206}Pb$ age of 1792 ± 12 Ma (Fig. 6d). A second age group, centered around ca. 1725 Ma, is derived from analyses of monazite 4 (B, C, and D). The second age group yields a nearly concordant mean age of 1724 ± 14 Ma and a weighted mean $^{207}Pb/^{206}Pb$ age of 1727 ± 15 Ma (Fig. 6e).

4.3.4. Western granulite facies, CC-601, metapelite

The sample of metapelite from the western granulite-facies zone (CC-601) is coarse grained, migmatitic, and contains Qtz + Bt + Kfs + Crd + Pl + Grt + Sil (Couëslan and Pattison, 2012).

appears truncated by the grain margin, and the monazite appears embayed; (f) back-scattered electron image of monazite G2, sample 108-08-226. The rounded grain margin at the bottom of the image truncates diffuse concentric zoning of the monazite; (g) back-scattered electron image of monazite 3, ferruginous metawacke sample CC-803, eastern granulite-facies zone. The idioblastic monazite displays concentric zoning; and (h) photomicrograph in reflected light of monazite 4, sample CC-803. The granoblastic monazite is optically continuous with a thin overgrowth of monazite along the grain boundary of the apatite.

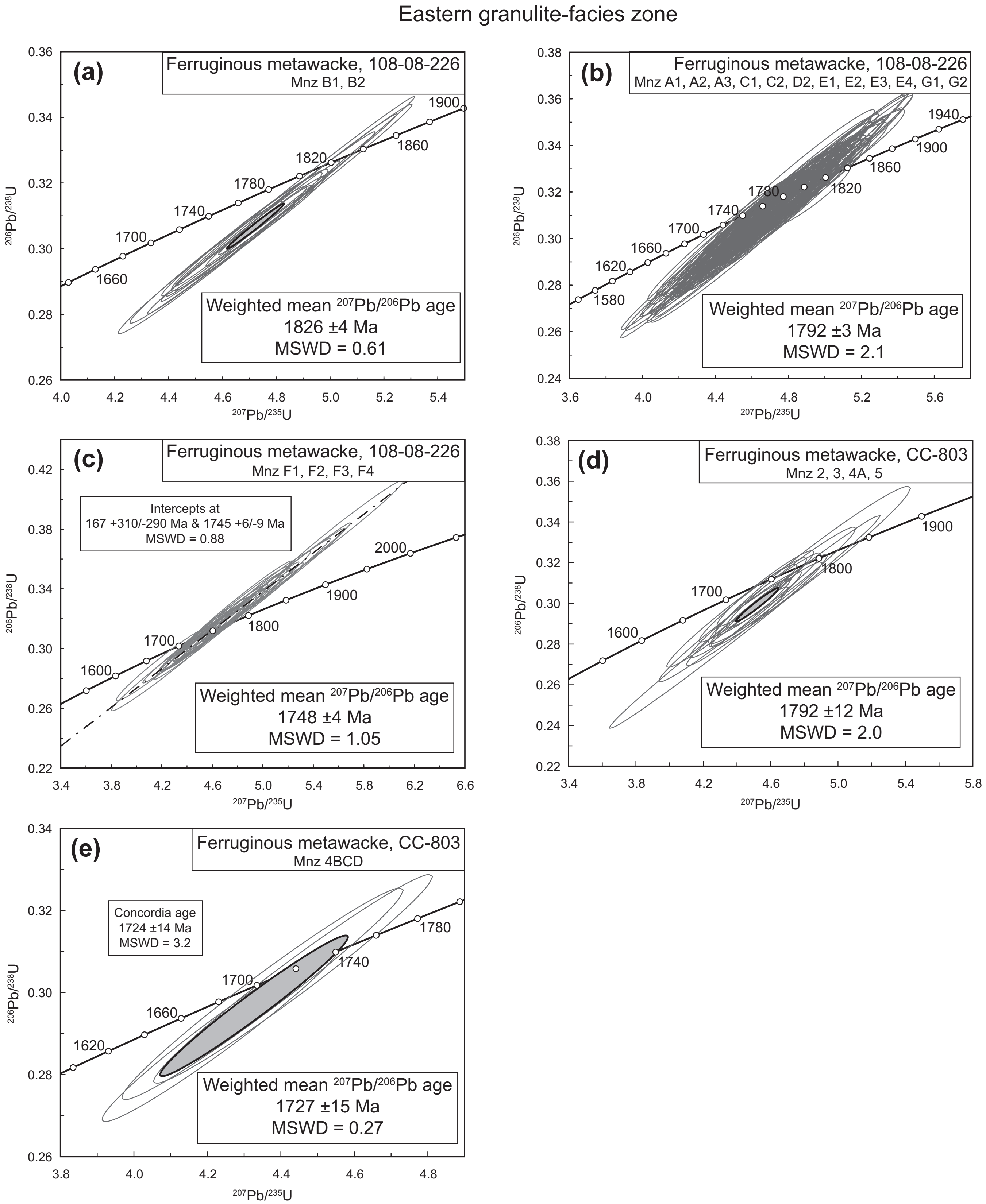

Fig. 6. U–Pb laser ablation results of metamorphic monazite from samples of metawacke from the eastern granulite-facies zone. Three different age groups were calculated for the sample 108-08-226 (a), (b), and (c), and two age groups were calculated for sample CC-803 (d) and (e). See text for discussion.

Veins of leucosome are oriented subparallel to S_2 but are not foliated. They consist of quartz, K-feldspar, and plagioclase with subordinate biotite, graphite, pyrrhotite, garnet, and cordierite. Acicular to prismatic sillimanite, biotite, and graphite are aligned along S_2 in the melanosome and occur as inclusions in garnet. The garnet, which forms coarse-grained poikiloblasts, is also wrapped by, and elongate parallel to, S_2.

Eight grains of monazite were analyzed, with three to seven spots analyzed per grain. Monazite grains 1 and 3 are subequant to tabular and occur within the matrix of the leucosome. Zoning in BSE images is complex and patchy with sharp domain boundaries (Fig. 7a). The undulating margin of grain 3 appears to truncate the zoning, and could indicate monazite dissolution. Monazite grain 2 is poikiloblastic and intergrown with prismatic sillimanite that is oriented parallel to S_2 (Fig. 7b). Zoning is complex but on the whole consists of a bright interior with darker margins. Monazite grains 4 and 5 are inclusions in a coarse-grained, poikiloblastic garnet, and occur along inclusion trails that are subparallel to S_2. Zoning of these monazite grains is diffuse and irregular (Fig. 7c). Monazite grains 6, 7, and 8 are granoblastic grains that occur within the matrix of the melanosome. Monazite 6 and 8 are enclosed by biotite and characterized by domainal zoning similar to monazite 1 and 3. Monazite 6 is intergrown with S_2 graphite and biotite (Fig. 7d). Monazite 7 is a relatively large monazite grain (~300 μm long) enclosed in cordierite and oriented parallel to S_2. It is characterized by diffuse zoning consisting of a generally brighter core and with darker zones toward the grain periphery (Fig. 7e).

The $^{207}Pb/^{206}Pb$ ages calculated for monazite from sample CC-601 range from ca. 1838 to 1777 Ma (Appendix A). The results appear to define a single age population with sufficient spread of the data to define a discordia with an upper intercept of 1812 ± 7 Ma (Fig. 8a). The weighted mean $^{207}Pb/^{206}Pb$ age of 1803 ± 5 Ma is identical within error.

4.3.5. *Western granulite facies, CC-602, meta-iron formation*

The sample of meta-iron formation is coarse grained and granoblastic, containing the metamorphic assemblage Opx + Qtz + Bt + Grt + Kfs (Couëslan and Pattison, 2012). Although the presence of orthopyroxene is not diagnostic of granulite-facies conditions for iron formations, textural evidence suggests that biotite was unstable and the majority of K-feldspar formed from the incongruent melting of biotite (Couëslan and Pattison, 2012). K-feldspar occurs as perthitic interstitial grains that are commonly partially replaced by skeletal quartz–biotite intergrowths. Interstitial grains of K-feldspar and quartz commonly display terminations with dihedral angles of approximately 20° (Fig. 7f). These interstitial grains resemble pseudomorphs of melt films as described by Harte et al. (1991), Hartel and Pattison (1996), Sawyer (1999), and Holness and Sawyer (2008). Orthopyroxene is typically slightly elongate parallel to S_2, and when spatially associated with K-feldspar can be partially overprinted by skeletal intergrowths of quartz and biotite with or without garnet. Biotite defines a weak S_2 foliation.

Two grains of monazite yielded reliable results, with one and three spots analyzed per grain. Monazite 1 is an equant, round inclusion within orthopyroxene. It is rimmed by a halo of metamict orthopyroxene 10–20 μm thick. A BSE image reveals a core characterized by oscillatory zoning and slightly elevated Th, rimmed by a darker overgrowth (Fig. 7g). The oscillatory zoning is most defined at the core of the grain, and becomes progressively less well defined or faded toward the darker overgrowth. Monazite grain 4 is a small unzoned and equant grain associated with what is interpreted as a quartz pseudomorph after melt (Fig. 7h).

The ages of monazite grains from sample CC-602 appear to record two periods of monazite growth. Monazite 4 and the core of monazite 1 (1A) yield $^{207}Pb/^{206}Pb$ ages of ca. 1756 and 1744 Ma, respectively (Appendix A). Two analyses from the outer portions of monazite 1 (1B and D) both yield a $^{207}Pb/^{206}Pb$ age of ca. 1703 Ma. The older age population yields a mean concordant age of 1752 ± 19 Ma and an identical mean $^{207}Pb/^{206}Pb$ age (Fig. 8b), while the data from the younger age group defines a concordant age of 1699 ± 25 Ma and a weighted mean $^{207}Pb/^{206}Pb$ age of 1703 ± 27 Ma (Fig. 8c).

5. Discussion

5.1. *Summary of previously reported ages*

Fig. 9 is a summary of previous U–Pb and $^{40}Ar/^{39}Ar$ geochronology analyses from the TNB and $^{207}Pb/^{206}Pb$ monazite ages from this study. The data set is heavily weighted toward rocks collected from the upper amphibolite-facies zone. This spatial bias is likely related to the predominance of upper amphibolite-facies rocks in easily accessible parts of the TNB, and the location of the Thompson mine within the upper amphibolite-facies zone. Magmatic intrusions are grouped according to the their tectonic significance as interpreted by the authors of each study, with the exception of data presented in Machado et al. (2011a,b). In these two studies, the authors interpret most structures in the TNB to be related to a period of long-lived transpression. Where possible, the observations of Machado et al. (2011a,b) have been re-interpreted assuming the deformation history outlined in Section 2.3 of this paper.

Pre-D_2 intrusions consist mostly of ultramafic rocks and contemporaneous felsic intrusions that cluster around 1880 Ma (Fig. 9, Percival et al., 2004, 2005; Hulbert et al., 2005; Heaman et al., 2009; Scoates et al., 2010). The data also includes a younger mafic dyke from the Thompson mine (ca. 1861 Ma, Scoates et al., 2010). Many of the mafic and ultramafic intrusions are interpreted as sills which were intruded conformably into Ospwagan Group rocks prior to the development of F_2 nappes (Bleeker, 1990a; Bleeker and Macek, 1996).

Pre- to syn-D_2, and syn-D_2 magmatic intrusions range in age from ca. 1851 to 1772 Ma and consist of larger felsic plutons and smaller granite and pegmatitic granite sheets and dykes which are foliated parallel to, and often concordant with, S_2 (Fig. 9, Bleeker et al., 1995; Zwanzig et al., 2003; Percival et al., 2004; Machado et al., 2011a,b). The ages of intrusions interpreted to be syn- to post-D_2, but pre-D_3, are relatively scattered between ca. 1798–1726 Ma (Machado et al., 1990, 2011a,b). They consist of pegmatitic granite dykes and sheets that are undeformed and intrude along S_2, and unfoliated dykes folded by F_3. The significant overlap with the ages of syn-D_2 intrusions suggests that many of these pre-D_3 intrusions are in fact syn-D_2. Magmatism appears to have been relatively continuous from ca. 1851 to 1770 Ma.

Syn-D_3 intrusions (Fig. 9) consist of two granitic pegmatite dykes. One of the dykes (ca. 1772 Ma) is reported to be axial planar to an F_3 fold (Machado et al., 2011a), the other dyke (ca. 1770 Ma) is part of a swarm that cross cuts the axial plane of a regional F_3 structure and is interpreted to be late D_3 (Bleeker, 1990a). The ages of these syn-D_3 intrusions are identical to the youngest intrusions interpreted as syn-D_2. This could suggest that the change from convergent (D_2) deformation to transpressive (D_3) deformation represents a continuous, progressive change in deformation style rather than two discrete episodes. However, the identical age of dykes interpreted as D_2 and the dyke interpreted as late D_3 suggests that the tectonic significance of some of these intrusions, or the obtained ages, have been mis-interpreted. Interpreting emplacement ages of plutons in the TNB is typically complicated by significant discordance of zircon populations and large inherited zircon components (Machado et al., 2011b).

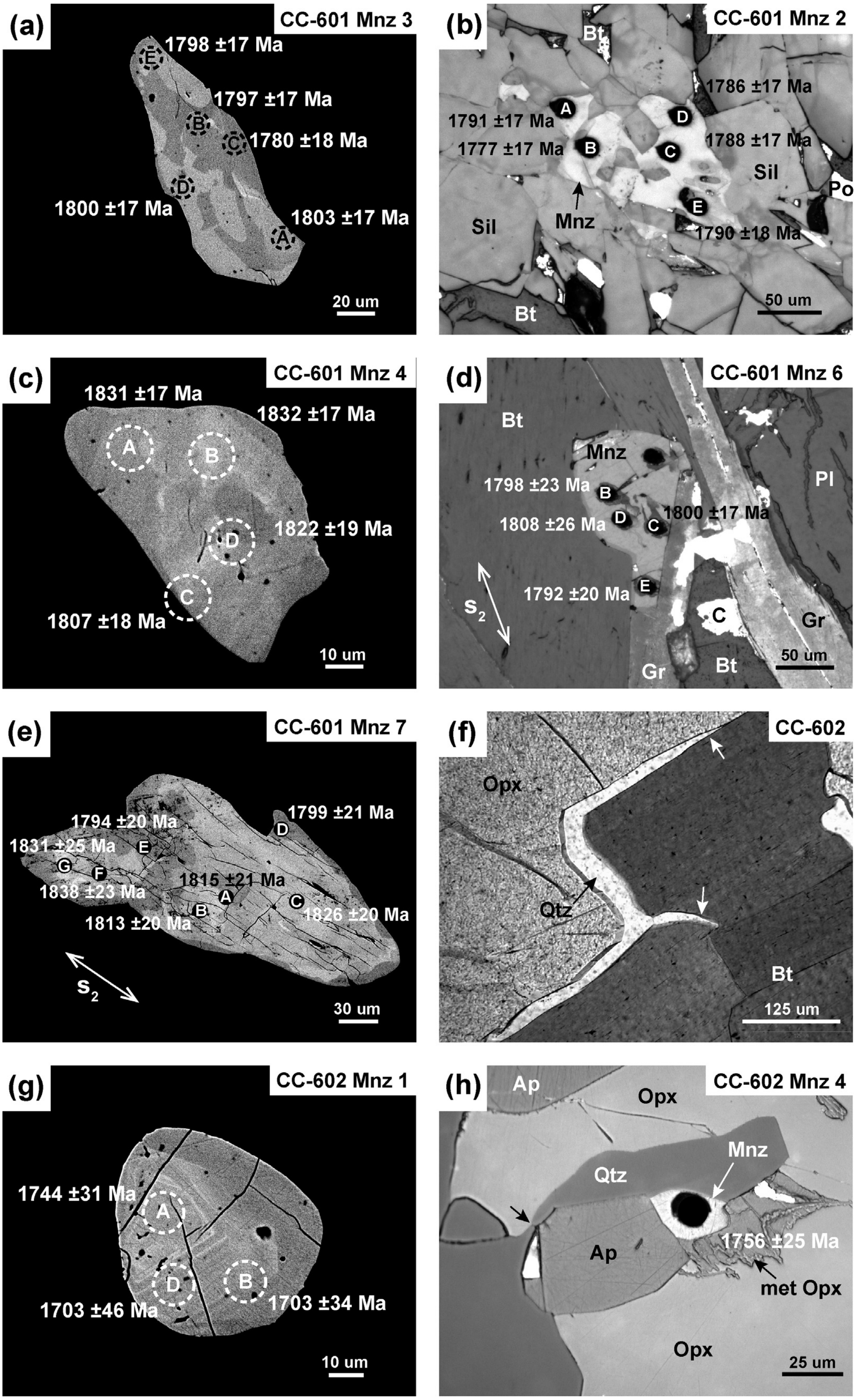

Fig. 7. (a) Back-scattered electron image of monazite 3, metapelite sample CC-601, western granulite-facies zone. The dashed circles indicate the locations of ablation pits along with the calculated $^{207}Pb/^{206}Pb$ ages; (b) photomicrograph in reflected light of monazite 2, sample CC-601. The monazite is intergrown with S_2 sillimanite; (c) back-scattered electron image of monazite 4, sample CC-601; (d) photomicrograph in reflected light of monazite 6, sample CC-601. The monazite is intergrown with S_2 biotite and graphite; (e) back-scattered electron image of monazite 7, sample CC-601; (f) photomicrograph in transmitted light of quartz pseudomorphous after an inter-granular melt-film in meta-iron formation sample CC-602. White arrows indicate the locations of low dihedral angles interpreted to represent solid-solid-pore space junctions

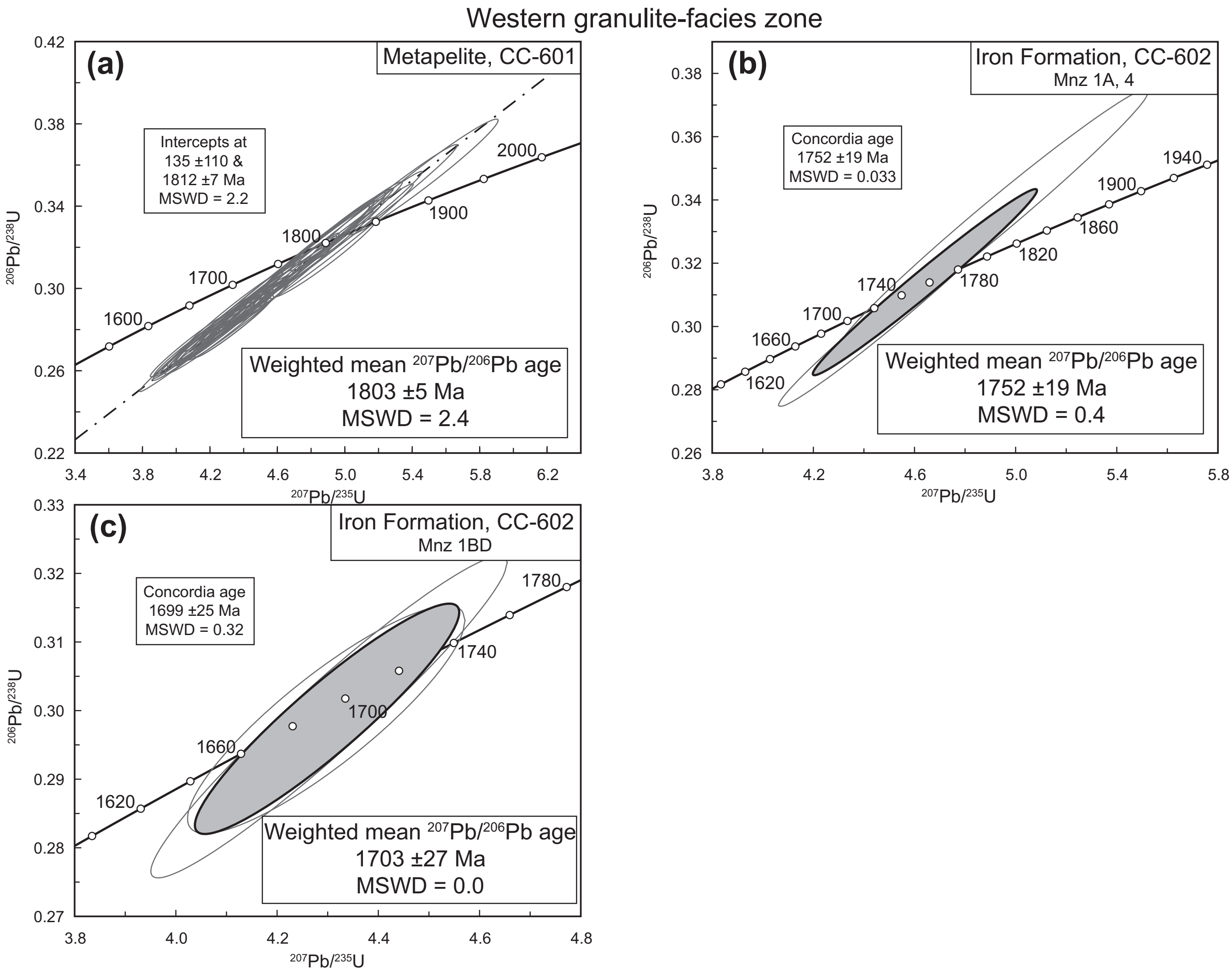

Fig. 8. U–Pb laser ablation results of metamorphic monazite from samples from the western granulite-facies zone, (a) metapelite sample CC-601, and (b) and (c) meta-iron formation sample CC-602. See text for discussion.

The ages obtained from metamorphic zircon and monazite have historically been interpreted to date the timing of peak metamorphism in the TNB. This has led to difficulty in interpreting the significant spread of ages recorded by metamorphic zircon and monazite (ca. 1810–1750 Ma, Fig. 9, Machado et al., 1990, 2011a; Rayner et al., 2006; Schneider et al., 2007; Burnham et al., 2009; Heaman et al., 2009). It is likely that this spread of metamorphic ages is the result of different periods of zircon and monazite growth along the metamorphic P–T paths of various rocks. Some ages are likely related to prograde metamorphic reactions such as the breakdown of allanite (Wing et al., 2003; Janots et al., 2007; Tomkins and Pattison, 2007; Spear, 2010; Gasser et al., 2012), while others are related to leucosome crystallization along the cooling paths of migmatitic rocks (Kelsey et al., 2008; Gasser et al., 2012). Still other ages could be related to thermal pulses associated with magmatism or episodes of hydrothermal overprinting not recognized by previous authors.

Schneider et al. (2007) reported on $^{40}Ar/^{39}Ar$ dating of hornblende, muscovite, and biotite in the TNB from north of Moak Lake to the south end of Setting Lake (Fig. 2). Hornblende ages ranged from ca. 1745 to 1723 Ma, biotite ages ranged from ca. 1789 to 1701 Ma, and a single muscovite analysis gave an age of ca. 1770 Ma. Assuming a closure temperature of 470 °C for muscovite and 330 °C for biotite (Baxter, 2010), the older ages are at odds with the ages obtained for hornblende (closure temperature of approximately 560 °C, Baxter, 2010) and with the monazite ages obtained in this paper. Much of the biotite and the muscovite $^{40}Ar/^{39}Ar$ data presented by Schneider et al. (2007) is characterized by either anomalous concentrations of K_2O, hump-shaped age spectra, or both. In addition, some biotite ages are significantly older than biotite and hornblende ages from immediately adjacent samples. In order to re-interpret the data it was filtered using the following criteria: typical muscovite and biotite contain 8–12 wt% K_2O (Fleet, 2003), therefore all muscovite and biotite analyses with K_2O <8% and >12% were ignored; and all $^{40}Ar/^{39}Ar$ analyses with a MSWD >4 for the age spectra were ignored. Two hornblende and three biotite analyses are found to satisfy these constraints (Fig. 9). The hornblende samples are from the upper amphibolite-facies

(Holness and Sawyer, 2008); (g) back-scattered electron image of monazite 1, meta-iron formation sample CC-602, western granulite-facies zone. Note the fine oscillatory zoning which becomes increasingly diffuse toward the dark rim of the grain; and (h) photomicrograph in reflected light of monazite 4, sample CC-602. The adjacent quartz may be pseudomorphous after intergranular melt. The black arrow marks where the melt film was necked-down between adjacent solid phases. The orthopyroxene adjacent to the monazite is metamict. *Abbreviations*: C, carbon coating residue from electron microprobe analysis; met Opx, metamict orthopyroxene.

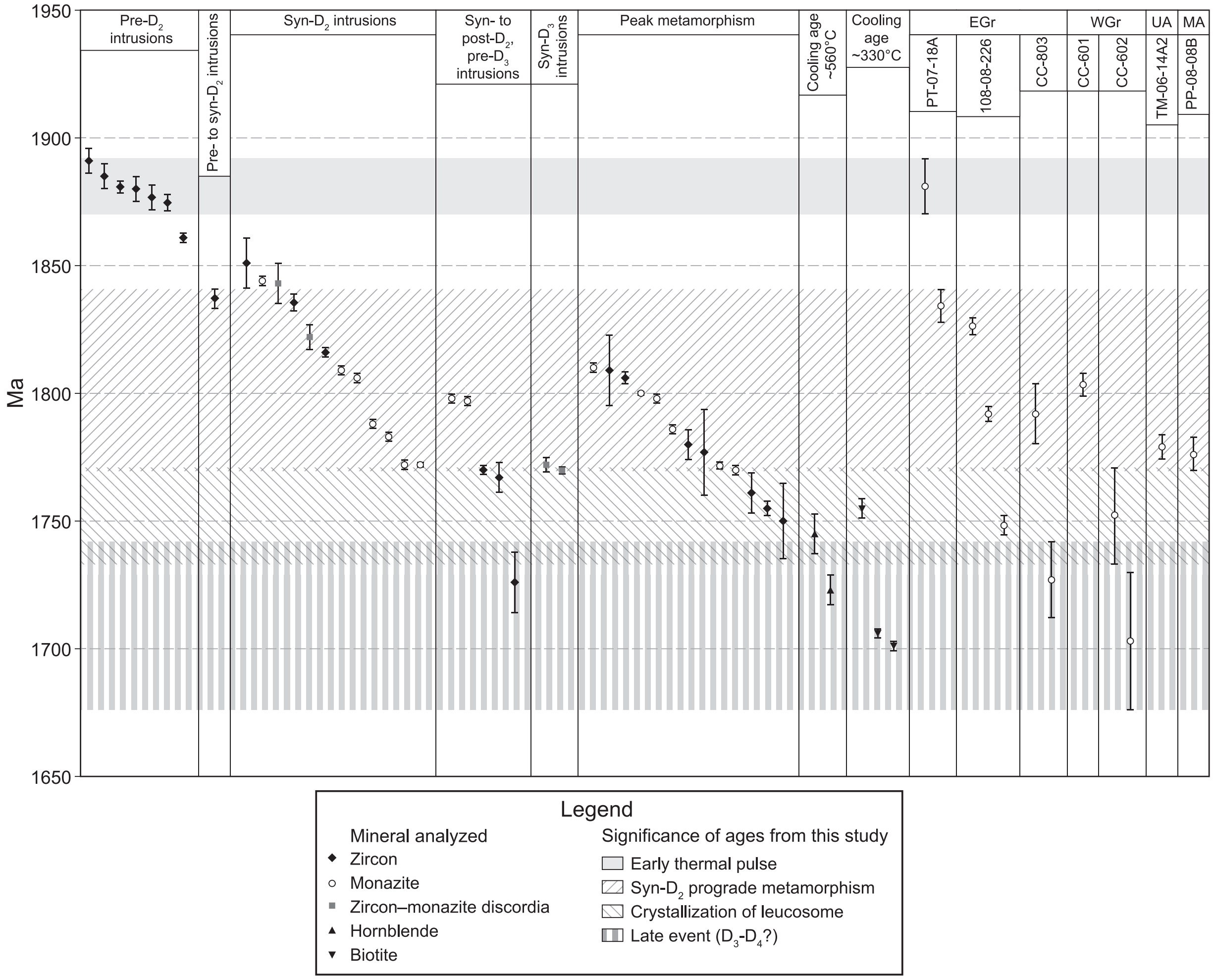

Fig. 9. Summary of U–Pb and $^{40}Ar/^{39}Ar$ ages from the TNB (Bleeker, 1990a; Machado et al., 1990, 2011a,b; Bleeker et al., 1995; Zwanzig et al., 2003; Percival et al., 2004, 2005; Hulbert et al., 2005; Rayner et al., 2006; Schneider et al., 2007; Burnham et al., 2009; Heaman et al., 2009; Scoates et al., 2010; this study).

and eastern granulite-facies zones and yielded ages of 1745 ± 8 Ma and 1723 ± 6 Ma, respectively (Schneider et al., 2007). The three biotite analyses were from the middle amphibolite-facies, upper amphibolite-facies, and eastern granulite-facies zones, and yielded ages of 1755 ± 4 Ma, 1706 ± 2 Ma, and 1701 ± 2 Ma, respectively (Schneider et al., 2007). Although it is limited, the $^{40}Ar/^{39}Ar$ data for the TNB suggest a pattern of older ages occurring in the zones of lower metamorphic grade and younger ages occurring in the zones of higher metamorphic grade.

5.2. Timing of metamorphism and deformation

Table 1 summarizes the timing of monazite crystallization and textural relationships in each sample from this study. Equilibrium-assemblage diagrams (Figs. 10 and 11) are used to relate the timing of monazite crystallization to metamorphic P–T paths for each sample. The bulk compositions used to calculate the equilibrium-assemblage diagrams and the position of the P–T paths are presented in Couëslan and Pattison (2012), and the reader is referred to that paper for details. In the discussion below, simplified reactions involving the key silicate phases in the metapelite samples come from Yardley (1989) and Spear (1993).

The timing of monazite crystallization during metamorphic events has been the subject of numerous studies. Petrological and thermodynamic studies in rocks of metapelitic bulk compositions suggest most prograde metamorphic monazite forms from the breakdown of allanite under lower to middle amphibolite-facies conditions (Kingsbury et al., 1993; Foster and Parrish, 2003; Wing et al., 2003; Rasmussen et al., 2006; Yang and Pattison, 2006; Janots et al., 2007, 2008; Tomkins and Pattison, 2007; Spear, 2010; Gasser et al., 2012). The studies are in general agreement that this reaction occurs in close proximity (spatially, temporally, and in terms of temperature) to the first appearance of cordierite, staurolite, and aluminosilicate minerals. Pyle and Spear (2003) suggested that an earlier period of monazite growth could be related to the consumption of xenotime during the initial growth of garnet under lower amphibolite-facies metamorphic conditions; however, the volume of monazite produced is likely to be limited by the relatively low concentrations of LREE and Th in xenotime (Foster and Parrish, 2003). With increasing metamorphic grade, monazite is predicted to remain a stable phase in metapelitic bulk compositions until the onset of partial melting. Experimental work by Rapp and Watson (1986), Rapp et al. (1987), Montel (1993), and Wolf and London (1995) indicate that monazite is soluble in peraluminous granitic melts and that the solubility is correlated to increasing temperature and a_{H_2O}, and inversely correlated to alumina saturation and REE content of the melt. Thermodynamic modeling by Kelsey et al. (2008) suggested that anatexis in a typical pelite (containing ~170 ppm LREE) should lead to total dissolution of monazite above temperatures of ~750 °C; however, diffusion and melting experiments suggest that monazite grains >50 μm in diameter are likely to require upwards of 10 million years in direct contact with the

Table 1
Summary of mean ages and textural settings of dated monazite from each sample.

Sample# Composition	Zone	Monazite $^{207}Pb/^{206}Pb$ age	Textural relations
PP-08-08B Pelite	MA	1776 ± 7 Ma	Included in late-S_2 garnet
TM-06-14A2 Pelite	UA	1779 ± 5 Ma	Included in garnet; monazite extensions parallel to S_2 biotite
		1881 ± 11 Ma	Included in garnet; enclosed by biotite in melanosome
PT-07-18A Pelite	E-Gr	1834 ± 7 Ma	Included in garnet; intergrown with sillimanite that is pseudomorphous after S_2 parallel andalusite
		1826 ± 4 Ma	Elongate parallel S_2, embayed grain boundaries
108-08-226 Ferruginous wacke	E-Gr	1792 ± 3 Ma	Elongate parallel S_2; embayed grain boundaries; partially overgrown by orthopyroxene, rare inclusions in Kfs
		1748 ± 4 Ma	Granoblastic monazite
CC-803 Ferruginous wacke	E-Gr	1792 ± 12 Ma	Idioblastic monazite, elongate parallel to S_2, concentric zoning
		1727 ± 15 Ma	Forms partial overgrowth on apatite
CC-601 Pelite	W-Gr	1803 ± 5 Ma	Associated with S_2 parallel inclusion trails in garnet; embayed grain boundaries; elongate parallel to S_2, intergrown with S_2 sillimanite, biotite, and graphite
CC-602 Iron formation	W-Gr	1752 ± 19 Ma	Inclusion in orthopyroxene, oscillatory zoning; associated with melt pseudomorphs
		1703 ± 27 Ma	Inclusion in orthopyroxene, zone of faded oscillatory zoning

Abbreviations: E-Gr, eastern granulite-facies zone; MA, middle amphibolite-facies zone; UA, upper amphibolite-facies zone; W-Gr, western granulite-facies zone.

melt for complete dissolution (Rapp and Watson, 1986; Montel, 1993; Wolf and London, 1995). It would not be unexpected then for large monazite grains, or those armored by refractory minerals, to survive an anatectic event. Whether partial or complete dissolution of monazite occurs during anatectic melting, crystallization of the melt during cooling should result in monazite growth as predicted by Pyle and Spear (2003), Kelsey et al. (2008), Spear and Pyle (2010), and Gasser et al. (2012).

5.2.1. *Eastern granulite-facies zone*

Monazite grains from the Paint Lake metapelite (PT-07-18A) yield two distinct age groups of 1881 ± 11 and 1834 ± 7 Ma (Fig. 9). The ca. 1881 Ma age group consists of complexly zoned monazite grains that typically occur as inclusions in garnet porphyroblasts; however, one monazite belonging to this group occurs enclosed by biotite in the melanosome. The monazite grains occur close to the margin as well as at the core of the large garnet porphyroblasts, suggesting they pre-date much of the garnet growth history (Fig. 3d). Monazite from the younger age group, ca. 1834 Ma, occurs intergrown with sillimanite that pseudomorphously replaced andalusite, and is present alongside staurolite and sillimanite in inclusion-rich zones of garnet porphyroblasts. These textures suggest monazite crystallization occurred at middle amphibolite-facies conditions during the prograde metamorphism of the metapelite (Fig. 10a).

The monazite from the Paint Lake metawacke, 108-08-226, yields three discrete age groups, 1826 ± 4, 1792 ± 3, and 1748 ± 4 Ma (Fig. 9). The alignment of one of the monazite grains of the oldest group (ca. 1826 Ma) parallel to S_2 suggests crystallization during D_2, and the embayed nature of the grain boundaries of monazite from this group suggest that the grains were subjected to dissolution during their history. The age of the oldest group of monazite is identical within error of the 1834 ± 7 Ma age monazite from pelite sample PT-07-18A, which suggests growth under approximately middle amphibolite-facies conditions. The largest population of monazite is from the ca. 1792 Ma age-group and includes grains in the metawacke groundmass that are elongate parallel to S_2, grains in the leucosome that are embayed, grains that have been partially overgrown by orthopyroxene porphyroblasts in the leucosome, and a single grain that was included in a K-feldspar porphyroblast in the leucosome. These relationships suggest that the monazite grew during D_2, was present during the growth of orthopyroxene, and was unstable in the leucosome and subject to partial dissolution. This restricts the monazite growth to metamorphic conditions down-grade of significant melt generation (Fig. 10a).

The most common reactant phase for monazite is allanite (Foster and Parrish, 2003; Wing et al., 2003; Tomkins and Pattison, 2007; Janots et al., 2008; Spear, 2010; Gasser et al., 2012). The proportions of Ca, Na, Al, and Fe in the bulk composition can have a significant impact on the stability of allanite during metamorphism. Allanite is predicted to remain stable to higher temperatures in metapelites with higher Ca, Fe, and Al contents (Foster and Parrish, 2003; Wing et al., 2003; Spear, 2010), and Janots et al. (2008) linked higher bulk rock CaO/Na_2O ratios to the preservation of allanite at higher temperatures. Metawacke samples 108-08-226 and CC-803 have higher bulk CaO/Na_2O ratios (1.19 and 1.01, respectively) compared to the metapelites in this study (0.52–0.60, Couëslan and Pattison, 2012). Therefore, it is possible that allanite remained stable into middle to upper amphibolite-facies metamorphic conditions (Fig. 10a, Bingen and van Breemen, 1998; Gasser et al., 2012). Monazite of the youngest group (ca. 1748 Ma) occurs within schlieric material at the boundary between the metawacke and the leucosome. The granoblastic textures of these grains suggest equilibrium with the surrounding matrix at the time of crystallization.

Monazite grains from the Phillips Lake metawacke, CC-803, yields two discrete age groups, 1792 ± 12 and 1727 ± 15 Ma (Fig. 9). The alignment of the idioblastic monazite from the oldest age group (ca. 1792 Ma) parallel to S_2 suggests crystallization during D_2, and by extension, during prograde metamorphism (Couëslan and Pattison, 2012). This age is identical to the main population of monazite from metawacke sample 108-08-226. The younger monazite age group of ca. 1727 Ma remains enigmatic. This age is derived from relatively Y-enriched portions of a monazite grain, which is typical of monazite growth coinciding with garnet dissolution (Kelly et al., 2006; Gasser et al., 2012) possibly during retrograde decompression (Foster and Parrish, 2003).

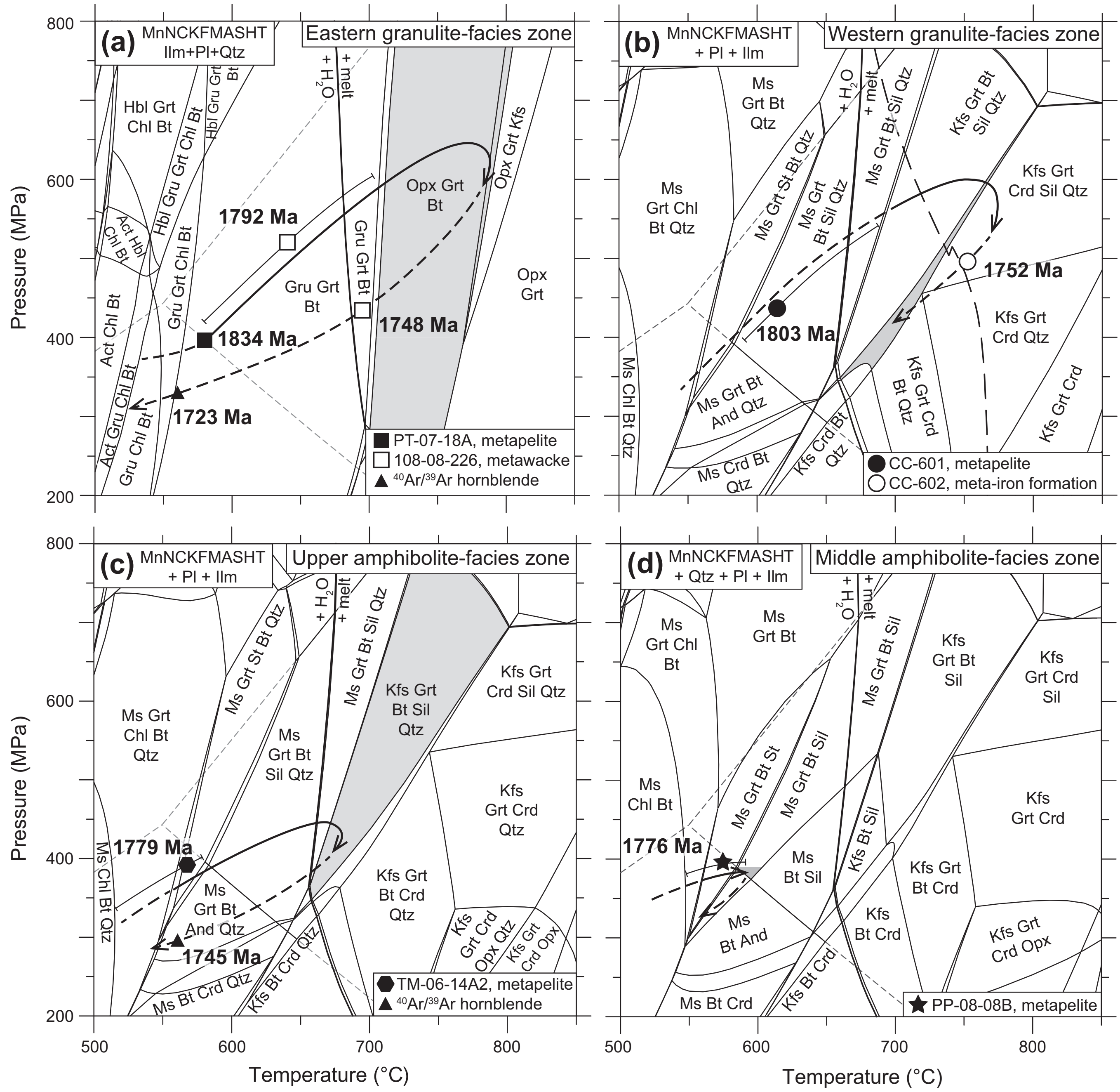

Fig. 10. Equilibrium-assemblage diagrams and interpreted metamorphic P–T–t paths for samples from the four metamorphic-facies zones. Equilibrium assemblage diagrams for (a) ferruginous metawacke 108-08-226, eastern granulite-facies zone, and (b) average Pipe Formation metapelite with P–T path for the western granulite-facies zone. The long dashed curve in (b) represents the solidus for meta-iron formation CC-602. Equilibrium assemblage diagrams for (c) metapelite TM-06-14A2, upper amphibolite-facies zone, and (d) metapelite PP-08-08B, middle amphibolite-facies zone. Symbols indicate the interpreted P–T conditions of monazite growth in samples from this study. Error bars associated with some symbols indicate the limits of possible monazite growth as inferred from textural relationships. $^{40}Ar/^{39}Ar$ hornblende ages in (a) and (c) are from Schneider et al. (2007). Dashed portions of P–T–t paths are inferred. Gray fields represent the observed metamorphic assemblages. Bulk compositions and P–T–t paths are from Couëslan and Pattison (2012). The dashed gray lines indicate the aluminosilicate stability-fields in the system $Al_2O_3–SiO_2–H_2O$, as defined by Holland and Powell (1998) based on Pattison (1992).

5.2.2. *Western granulite-facies zone*

Monazite grains from the Pipe Formation metapelite sample CC-601 (drill hole northwest of Thompson) yielded an age of 1803 ± 5 Ma (Fig. 9). Monazite grains are present in the matrix of the leucosome and melanosome, they occur as intergrowths with S_2 parallel sillimanite, biotite, and graphite, and are commonly elongate parallel to S_2. Monazite is also associated with S_2 inclusion trails in poikiloblastic garnet. The intergrowth textures observed between monazite and sillimanite suggests contemporaneous growth of the two phases (Fig. 7c).

There are two major sillimanite-forming reactions that likely affected this rock. First is the staurolite-consuming reaction that occurs in middle amphibolite-facies assemblages (Fig. 11b):

$$Ms + St + Qtz = Al_2SiO_5 + Bt + Grt + H_2O. \quad (1)$$

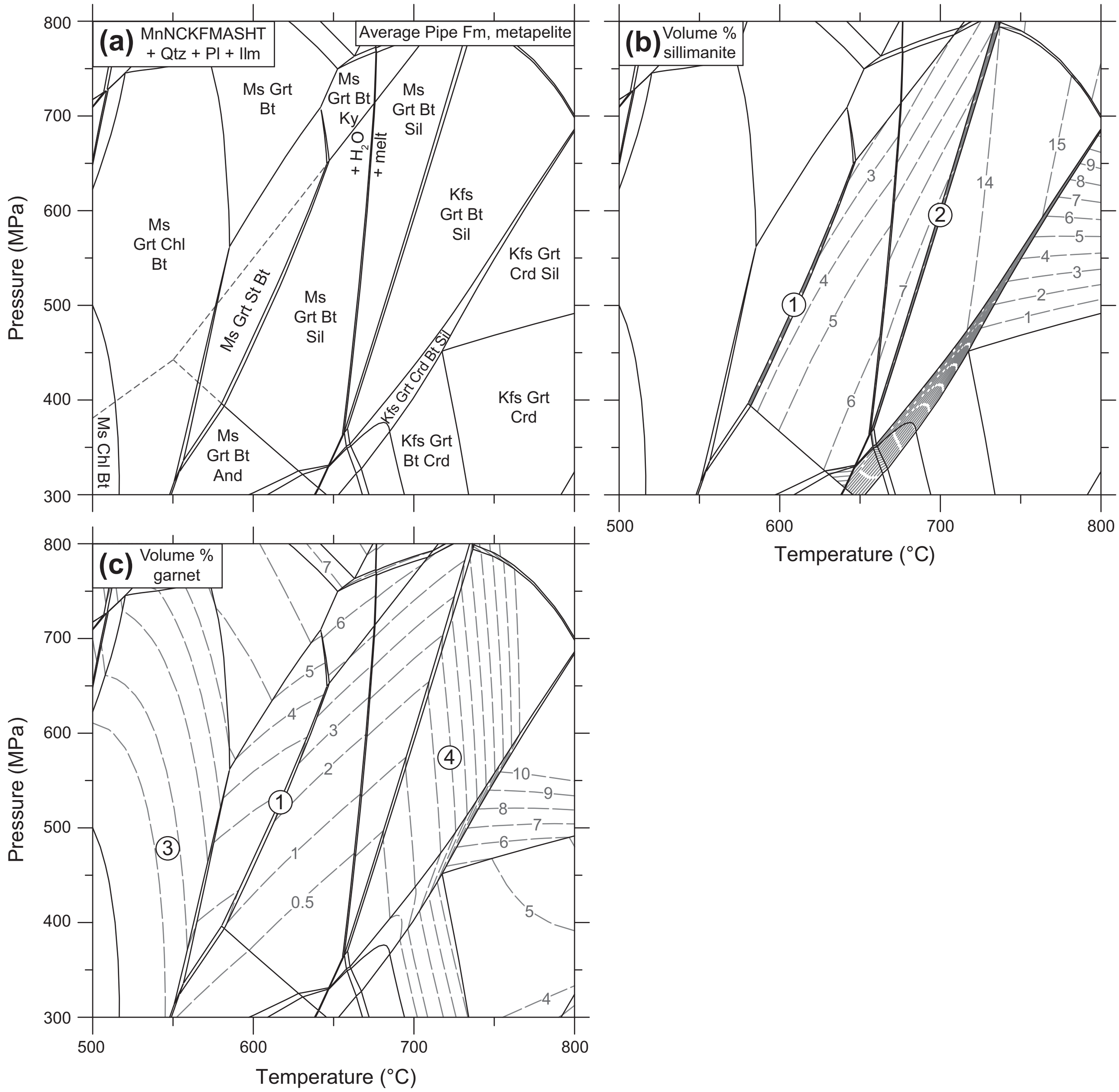

Fig. 11. (a) Equilibrium-assemblage diagram for average Pipe Formation metapelite (Couëslan and Pattison, 2012). The dashed gray lines indicate the aluminosilicate stability-fields in the system Al_2O_3–SiO_2–H_2O, as defined by Holland and Powell (1998) based on Pattison (1992). Isopleths for (b) volume % sillimanite, and (c) volume % garnet are overlain on the equilibrium-assemblage diagram of (a). The numbered fields and phase boundaries correspond to metamorphic reactions discussed in the text.

The second major sillimanite-forming reaction is the incongruent melting of muscovite at upper amphibolite-facies conditions (Fig. 11b):

$$\text{Ms} + \text{Qtz} \pm \text{Pl} = \text{Sil} + \text{melt} \pm \text{Kfs}. \quad (2)$$

Fig. 11b shows that sillimanite growth is predicted to be continuous between reactions (1) and (2). The intergrowth of monazite and sillimanite effectively brackets the growth of the monazite to metamorphic conditions between the onset of reaction (1) and the termination of reaction (2). Dissolution textures of some monazite within the leucosome matrix suggest the monazite was unstable in the presence of melt, and therefore unlikely to have grown during reaction (2) as melt was produced. Therefore, the preferred interpretation is that the monazite crystallization was coincident with D_2, and occurred at metamorphic conditions of middle amphibolite-facies (Fig. 10b). The large size of the leucosome-hosted monazite (>100 μm) likely prevented their complete dissolution into the surrounding silicate melt.

Meta-iron formation sample CC-602 occurs 15 m down hole from metapelite sample CC-601, so it will have experienced a similar metamorphic history. However, the monazite ages obtained from sample CC-602 yield two age groups that are significantly younger (Fig. 9). The older age group, 1752 ± 19 Ma, is derived from an oscillatory zoned grain and an unzoned grain that is associated with a possible quartz melt pseudomorph. Oscillatory zoning is considered characteristic of growth in a dynamic environment influenced by a magma or fluid (Shore and Fowler, 1996; Schaltegger et al., 1999). The ca. 1752 Ma age group is interpreted to represent the timing of melt crystallization along the retrograde segment of the metamorphic P–T path (approximately 750 °C, Fig. 10b). The younger, 1703 ± 27 Ma, age group is derived from analyses of the darker rim and an area of faded oscillatory zoning in monazite 1. Similar textures in zircon, of "ghosts" of oscillatory zoning, were attributed to solid state recrystallization by Hoskin and Black (2000). The ca. 1703 Ma age could therefore reflect a cryptic recrystallization event.

5.2.3. Upper amphibolite-facies zone

The Pipe Formation metapelite sampled from the Thompson mine (TM-06-14A2) yielded monazite with an age of 1779 ± 5 Ma (Fig. 9). Similar monazite ages of ca. 1773–1769 Ma were obtained by Rayner et al. (2006) for grain separates from a sample of Pipe Formation metapelite from the Thompson mine. Minor monazite growth parallel to S_2 biotite suggests at least some syn-D_2 growth, and monazite inclusions in garnet suggest monazite crystallization prior to, or during, a period of garnet growth. There are three major garnet-forming reactions in amphibolite-facies metapelites. The first reaction occurs under lower amphibolite-facies conditions and is responsible for the first appearance of garnet (Fig. 11c):

$$\text{Ms} + \text{FeMg-Chl} + \text{Qtz} = \text{Fe-Grt} + \text{FeMg-Bt} + \text{Mg-Chl} + H_2O. \quad (3)$$

The second garnet-forming reaction is reaction (1). The third period of garnet growth that likely affected this sample is a continuous reaction at upper amphibolite-facies conditions (Fig. 11c):

$$\text{Sil} + \text{FeMg-Bt} + \text{Qtz} = \text{Grt} + \text{Mg-Bt} + \text{melt} \pm \text{Kfs}. \quad (4)$$

The inclusion of monazite grains in garnet therefore only constrains monazite growth to metamorphic conditions coincident with, or down-grade of, reaction (4). However, reactions (1) and (4) produce less garnet modally than reaction (3), and generally result in rims and overgrowths on pre-existing garnet formed at lower grade such as by reaction (3). Combined with the constraints for monazite growth as outlined at the start of this section, our preferred interpretation is that the monazite grew during D_2 as the rock reached lower to middle amphibolite-facies conditions along the prograde segment of the rock's P–T path (Fig. 10c). This interpretation differs from that of Rayner et al. (2006), who interpreted monazite of similar age to have grown at peak conditions even though the reactions by which it was produced were not considered.

5.2.4. Middle amphibolite-facies zone

Monazite from the Pipe Formation metapelite sample PP-08-08B (Pipe II mine) yielded an age of 1776 ± 7 Ma (Fig. 9). The local presence of monazite as inclusions in garnet suggests it grew prior to, or concurrently with, a period of garnet growth. Reactions (1) and (3) are the only garnet producing reactions predicted to have affected this sample (Fig. 11c); therefore, reaction (1) places an upper bracket on the timing of monazite growth. This is in agreement with the previous assertions that the major interval of monazite growth in most metapelites is close to conditions of the incoming of staurolite, cordierite, and aluminosilicate minerals. The presence of staurolite in the sample suggests that reaction (1) did not proceed to completion and that garnet production may have been ongoing under peak metamorphic conditions. We therefore interpret the monazite to have grown during D_2 as the rock approached peak metamorphism at lower to middle amphibolite-facies conditions (Fig. 10d).

5.2.5. Summary and significance of monazite ages

The oldest monazite from metapelite sample PT-07-18A from the eastern granulite-facies zone yielded an age of 1881 ± 11 Ma, which coincides with a significant period of mafic and felsic magmatism in the TNB (Fig. 9, Heaman et al., 2009). It is possible that the timing of monazite growth is the result of a thermal pulse related to this period of magmatism.

Most samples from this study contain monazite populations interpreted to be contemporaneous with D_2 (ca. 1834–1776 Ma, Fig. 9). This period of syn-D_2 monazite growth correlates with the timing of syn-D_2 intrusions (ca. 1850–1770 Ma). It is not certain whether monazite growth was episodic and related to thermal pulses associated with increased periods of magmatism, or whether it was related to a single progressive metamorphic event. Magmatic ages suggest syn-D_2 magmatism was relatively continuous with no evidence for periods of increased activity (Fig. 9); however, two ages from the eastern granulite-facies zone appear to be relatively older (1834 ± 7 and 1826 ± 4 Ma), which could suggest a discrete thermal pulse. Similar ages were not recorded elsewhere in the belt, suggesting a localized event in the Paint Lake area. The remainder of syn-D_2 prograde metamorphic ages could indicate a more continuous progressive metamorphic event affecting the TNB from ca. 1803 to 1776 Ma.

The 1752 ± 19 Ma monazite from iron formation sample CC-602, western granulite-facies zone, is interpreted to date the timing of leucosome crystallization in this rock (Figs. 9 and 10b). A similar age of 1748 ± 4 Ma was obtained from a population of monazite in metawacke sample 108-08-226 from the eastern granulite-facies zone. This population of monazite crystallized in close spatial association with schlieric material at the boundary between metawacke and leucosome. A possible interpretation for these monazite grains is that they crystallized under similar conditions as the monazite from sample CC-602, both of these ages dating the crystallization of leucosome as the rocks cooled below their respective solidi (700–750 °C, Fig. 10a and b). The leucosome from metawacke sample 108-08-226 is massive and cross-cuts S_2 fabrics suggesting crystallization after the D_2 generation of deformation. Cooling was also ongoing elsewhere in the belt at this time as indicated by $^{40}Ar/^{39}Ar$ ages of hornblende from the upper amphibolite-facies zone (ca. 1745 Ma, Fig. 9) and biotite from the middle amphibolite-facies zone (ca. 1755 Ma, Schneider et al., 2007).

The significance of the youngest monazite ages from this study remains uncertain. The youngest monazite from metawacke sample CC-803 from the eastern granulite-facies zone (1727 ± 15 Ma), and iron formation sample CC-602 from the western granulite-facies zone (1703 ± 27 Ma) are both accompanied by large errors. They have considerable overlap with hornblende and biotite $^{40}Ar/^{39}Ar$ ages reported for the TNB (Fig. 9, Schneider et al., 2007), perhaps indicating crystallization during cryptic retrograde metamorphic events.

5.3. Tectonic model

5.3.1. Previous models

A summary of previous interpretations for the timing of deformation and metamorphism is presented in Table 2. Much of the tectonic history of the TNB remains contentious and significant disagreement exists between current tectonic models (cf. Percival et al., 2005; Burnham et al., 2009; Corrigan et al., 2009; Machado et al., 2011a).

The first evidence for tectonic activity along the formerly passive margin of the TNB is the widespread mafic and felsic magmatism at ca. 1890–1880 Ma. The magmatism could be related to a continental arc that formed along the Superior margin at ca. 1890 Ma as a result of the eastward subduction of Manikewan ocean crust under the craton (Percival et al., 2005; Corrigan et al., 2009). Mafic dykes of the Molson swarm, which parallel the craton margin, are interpreted to be the product of continental back-arc rifting (Percival et al., 2005; Zwanzig et al., 2007). Ansdell (2005) suggested that an unknown terrain collided with the Superior craton at ca. 1890 Ma, the collision causing the formation of D_1 structures that were then cut by the later Molson dykes at ca. 1880 Ma. The colliding terrain may have rifted away during a later period of extension related

Table 2
Previous interpretations for the approximate timing of deformation and metamorphism in the TNB. All ages are in Ma.

	D_1	D_2	D_3[a]	Peak met
Bleeker (1990b)	>1880	1822–1770	1770–1700	
White et al. (1994)		1820–1800		1790–1770
Bleeker and Macek (1996)	>1880		ca. 1770	1820–1780
White et al. (1999)	>1880		1800–1770	1820–1809
White et al. (2002)		ca. 1820	1800–1770	ca. 1820
Ansdell (2005)	ca. 1890	1840–?		ca. 1810
Percival et al. (2005)	>1883			
Percival et al. (2006)		1820–1790		
Rayner et al. (2006)				ca. 1770
Schneider et al. (2007)				1820–1800
Burnham et al. (2009)		>1818	ca. 1770	
Corrigan et al. (2009)		1830–?	1820–1770	
Machado et al. (2011a)		1890–1885	1850–1750 or 1720	1786–1750
Machado et al. (2011b)			ca. 1850	1805–1795

[a] Transpressional tectonics.

to the generation of the Winnipegosis komatiites (ca. 1864 Ma), which occur under Paleozoic limestone roughly 200 km south of the exposed TNB (Hulbert et al., 1994). Possible candidates for colliding terrains include fragments of Archean crust which may now underlie much of the northeastern Kisseynew Domain (Percival et al., 2005; Zwanzig et al., 2006); and the Snow Lake subdomain of the Flin Flon Domain where Nd-isotope geochemistry suggests relatively higher degrees of contamination by Archean-age crust, and where local sedimentary sequences contain detrital zircon similar in age to Superior crust (Bailes and Böhm, 2008; Corrigan et al., 2009).

In contrast to rifting processes, Heaman et al. (2009) suggested the mafic magmatism of the Molson swarm was the product of passive upwelling of the asthenosphere, with the intrusion of mantle-derived magmas occurring along the attenuated craton margin. In this model, the thermal pulse associated with the mantle upwelling and mafic magmatism induced melting of the continental crust and was responsible for the accompanying felsic magmatism. The authors also noted that a subduction-related trace-element signature is not present in the mafic rocks of the Molson swarm.

There was likely a close spatial association between the Superior craton and Reindeer Zone by ca. 1850–1840 Ma based on the similar age of felsic and mafic rocks emplaced in both tectonic elements, and the proposed age of the overlapping Grass River Group (Ansdell, 2005). Rocks exposed in structural culmination in the northeastern Kisseynew Domain and northwestern TNB suggests an early D_2 thrust sheet of Burntwood Group rocks was emplaced on top of the TNB, with the footwall detachment occurring near the middle of the Pipe Formation of the Ospwagan Group (Zwanzig and Böhm, 2002; Percival et al., 2006; Zwanzig et al., 2006). Terminal collision along this margin of the Superior craton, involving closure of the Manikewan ocean, is estimated at ca. 1840–1820 Ma (Table 2, White et al., 2002; Ansdell, 2005; Percival et al., 2006; Corrigan et al., 2009). This period of orogenesis may have led to the development of large D_2 nappe structures and high-grade metamorphism. The timing of peak metamorphism has been proposed over a range of intervals from ca. 1820 to 1770 Ma (Table 2).

Convergence is believed to have been greatest in the north along the Thompson Promontory which behaved as an indentor (Fig. 1, White et al., 2002; Kuiper et al., 2011; Couëslan and Pattison, 2012). Continued convergence during final stages of the collision may have generated D_3 sinistral and dextral transpressive shearing along the southwest and east sides of the promontory, respectively (White et al., 2002; Ansdell, 2005; Kuiper et al., 2011). A range of dates is proposed for the initiation and termination of D_3, with transpression beginning as early as ca. 1820 Ma (Table 2, Corrigan et al., 2009) and ending as late as ca. 1700 Ma (Bleeker, 1990b). Transpression led to the development of steeply east-dipping D_3–D_4 shear zones and upright F_3–F_4 folds.

The polarity of convergence remains a matter of debate. Juvenile plutons located in the Setting Lake area suggest eastward subduction of Manikewan ocean crust under the Superior craton margin at ca. 1840–1830 Ma (Bleeker et al., 1995; Zwanzig et al., 2003; Percival et al., 2005). Authors invoking this model have argued for the development of southwest-verging D_2 structures, and the thrusting of Superior craton rocks onto the Reindeer Zone (Zwanzig and Böhm, 2002; Zwanzig et al., 2006; Burnham et al., 2009). However, models by Ellis and Beaumont (1999) and White et al. (2002) preferred the westward subduction of the Superior craton margin under the Reindeer Zone. These models, based on the interpretation of seismic data, called for the initial formation of an east-verging fold-and-thrust belt on the Superior craton and west-verging structures within the Reindeer Zone. Rocks from the Superior margin were uplifted and translated westward toward the west-verging structures of the Reindeer Zone during the later sinistral transpression, and resulted in overprinting of the earlier east-verging structures (Ellis and Beaumont, 1999; White et al., 2002). A third model involving long-lived transpression was proposed by Gapais et al. (2005) and Machado et al. (2011a). It calls for west-verging D_3 transpressive tectonics to begin significantly earlier at ca. 1850 Ma. Transpression was initiated under high-grade metamorphic conditions, accompanied by anatexis, and continued during the subsequent retrogression until ca. 1750–1720 Ma.

5.3.2. New interpretations

No U–Pb ages from this study pre-date the mafic dykes that cross cut the Ospwagan Group stratigraphy and D_1 structures. The absence of older ages could suggest poor preservation of metamorphic monazite related to D_1, or it could suggest that the metamorphism accompanying D_1 was relatively low grade, such that metamorphic monazite did not crystallize. The latter interpretation is consistent with Zwanzig (1998) and Burnham et al. (2009), who suggested that D_1 was characterized by upright folding restricted to the Ospwagan Group cover sequence, and was not the main nappe-forming event as proposed by Bleeker (1990a). This is also supported by the ca. 1880 Ma ultramafic sills that are concordant with rocks of the Ospwagan Group and are characterized by magmatic layering that is consistent with the younging direction of the enclosing metasedimentary rocks. The lack of a recognized metamorphic event associated with D_1 is perhaps more consistent with the arc models of Percival et al. (2005) and Corrigan et al. (2009), than the collisional model for D_1 of Ansdell (2005) the latter which might be expected to generate a more significant metamorphic event. The asthenospheric upwelling model of

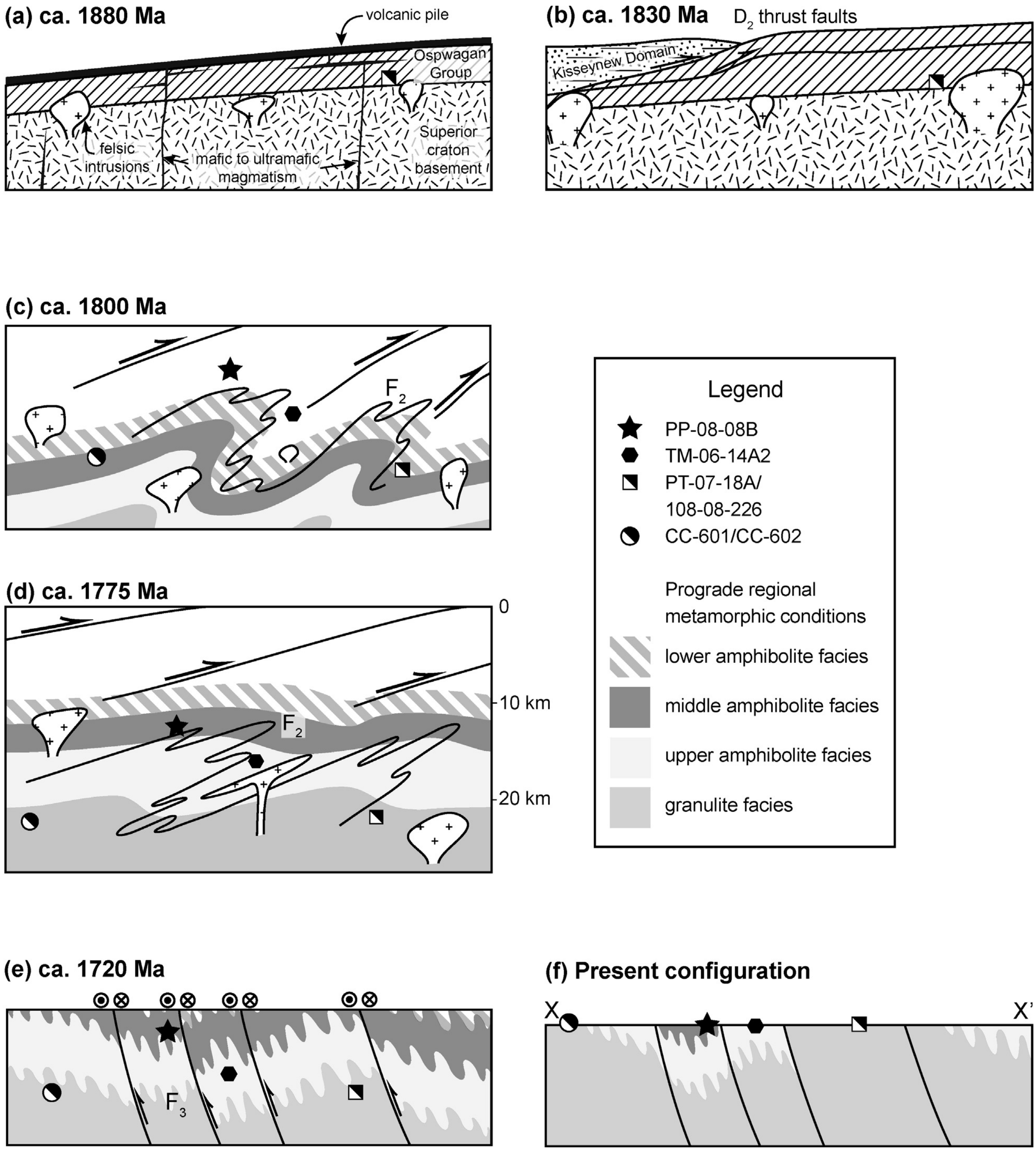

Fig. 12. A schematic model of the tectonic evolution of the Thompson Nickel Belt begins at (a) ca. 1880 Ma with mafic and felsic magmatism along the Superior craton margin. A thermal pulse related to the magmatism was recorded by sample PT-07-18A; (b) collision of the Reindeer Zone with the Superior craton at ca. 1830 Ma (early-D_2) resulted in thrusting of Kisseynew Domain rocks over TNB rocks. At approximately the same time, a local thermal event was recorded by samples PT-07-18A and 108-08-226, in the Paint Lake area; (c) continued convergence (D_2) and accompanying plutonism at ca. 1800 Ma. Rocks presently in the western granulite-facies zones (samples CC-601 and CC-602) attained metamorphic conditions of at least middle amphibolite-facies by this time. The vergence of F_2 folds in this schematic is arbitrary, models have been proposed for both west-verging nappes (Zwanzig et al., 2006) and east-verging nappes (White et al., 2002); (d) the later stages of D_2, ca. 1775 Ma, rocks presently in the middle amphibolite-facies zone (sample PP-08-08B) were approaching peak metamorphic conditions. The vertical scale is an approximation and not proportional to the horizontal direction; (e) by ca. 1720 Ma, transpressive tectonics are well underway (D_3). A $^{40}Ar/^{39}Ar$ age for hornblende reported by Schneider et al. (2007) suggest rocks presently exposed in the eastern granulite-facies zone were at ~560 °C. D_3 folding of metamorphic zones, and separation across ductile faults, is shown; and (e) the present day configuration of the metamorphic zones of the TNB is ascribed to differential uplift along D_3–D_4 structures. This schematic cross section is along line X–X′ in Fig. 2, samples are projected along strike for reference.

Heaman et al. (2009) may be equally valid with the findings of this study.

Interaction between the Superior craton and the Reindeer Zone was initiated by ca. 1850–1840 Ma. The early-D_2 thrusting of Burntwood Group rocks from the Kisseynew Domain over Superior craton rocks would have occurred sometime after ca. 1840 Ma, the approximate depositional age of the Burntwood Group. This was followed by crustal thickening in the form of nappe-like folding (F_2) and the development of the dominant S_2 foliation. D_2 was accompanied by relatively continuous magmatism, which may have resulted in heat advection and contributed to the high temperature – low pressure-style of regional metamorphism characteristic of the TNB. Data from this study suggest there may have been a thermal pulse in the eastern granulite-facies zone at ca. 1830 Ma (PT-07-18A and 108-08-226, Fig. 12b). This event attained at least middle amphibolite-facies conditions in the Paint Lake area. It is possible similar thermal events may have occurred elsewhere in the TNB.

A progressive regional metamorphic event is recorded in the TNB beginning with rocks that are now part of the western granulite-facies zone. These rocks were buried and subjected to at least middle amphibolite-facies conditions by 1803 ± 5 Ma (CC-601, Fig. 12c). Rocks that are now part of the eastern granulite-facies zone were subjected to at least middle amphibolite-facies conditions by 1792 ± 3 Ma (108-08-226). As crustal thickening continued, these rocks were buried to deeper crustal levels and subjected to higher metamorphic grades. Rocks that are now part of the upper and middle amphibolite-facies zones are interpreted to have attained lower to middle amphibolite-facies conditions by 1779 ± 5 and 1776 ± 7 Ma, respectively (TM-06-14A2 and PP-08-08B, Fig. 12d). This inferred process of progressive crustal thickening and the upward migration of metamorphic-facies isograds through the thickening pile may account for the observed pattern of older ages in rocks that attained the highest metamorphic grades and younger ages in rocks that attained lower metamorphic grade.

A change to transpressive tectonics in the TNB led to D_3 folding and faulting, accompanied by local metamorphic retrogression. Schneider et al. (2007) reported a $^{40}Ar/^{39}Ar$ biotite age of ca. 1755 Ma from the northern portion of the middle amphibolite-facies zone indicating the rocks had cooled to approximately 330 °C. At approximately the same time, 1752 ± 19 Ma, rocks now exposed in the western granulite-facies zone had cooled along their retrograde P–T path to near solidus conditions (approximately 750 °C, sample CC-602, Fig. 10b). Rocks in the eastern granulite-facies zone cooled to near solidus conditions by 1748 ± 4 Ma (approximately 700 °C, sample 108-08-226). A similar $^{40}Ar/^{39}Ar$ hornblende age of ca. 1745 Ma is reported by Schneider et al. (2007) for the upper amphibolite-facies zone, suggesting cooling through approximately 560 °C. Continued retrogression is recorded by an $^{40}Ar/^{39}Ar$ hornblende age of ca. 1723 Ma from the granulite-facies zone suggesting cooling to 560 °C (Fig. 12e), followed by biotite cooling ages from the upper amphibolite-facies zone and granulite-facies zones at ca. 1706 and 1701 Ma, respectively (Fig. 12f, Schneider et al., 2007).

The cooling pattern of rocks in the TNB suggests the lowest grade rocks cooled to approximately greenschist-facies temperatures relatively quickly, whereas rocks that attained the highest metamorphic grade record a more prolonged cooling path from temperatures close to the solidus to temperatures of greenschist-facies conditions. This cooling pattern is likely related to the differential uplift of crustal blocks during D_3–D_4 that resulted in the juxtaposition of zones of varying metamorphic grade (Couëslan and Pattison, 2012). From the limited data, cooling rates can be calculated for the Paint Lake area of the eastern granulite-facies zone and central portions of the upper amphibolite-facies zone. The Paint Lake area experienced average cooling rates of approximately 6 °C/m.y. from ca. 1748 to 1723 Ma and 11 °C/m.y. from ca. 1723 to 1701 Ma. The upper amphibolite-facies zone experienced an average cooling rate of approximately 6 °C/m.y. from ca. 1745 to 1706 Ma.

Although the data from this study do not resolve the question of vergence of the collision between the TNB and the Reindeer Zone, it does help constrain the timing of metamorphism and deformation within the belt. Our data suggests that the D_2 deformation event continued from ca. 1830 Ma to at least ca. 1776 Ma. Timing for the initiation of D_2 is in relatively good agreement with previous investigations (Table 2); however, we suggest D_2 was relatively long-lived similar to the findings of Bleeker (1990b). The $^{40}Ar/^{39}Ar$ data reported by Schneider et al. (2007) indicates that D_3-related uplift was underway by ca. 1755 Ma. This is supported by a similar age of ca. 1748 Ma for post-D_2 leucosome crystallization in the eastern granulite-facies zone. Combined D_3–D_4 transpression likely continued beyond ca. 1700 Ma. Estimates for the timing of D_3–D_4 deformation is later than most previous suggestions (Table 2), but again, is in relatively close agreement with the findings of Bleeker (1990b).

Regional metamorphism therefore appears to have occurred as a single progressive event, although it may have been punctuated by local thermal disturbances related to contemporaneous magmatism. This metamorphic event was recorded diachronously across the belt, depending on the metamorphic grade of the rocks that are now exposed. The interpretations from this study differ from the findings of Gapais et al. (2005) and Machado et al. (2011a), most significantly in showing that metamorphic grade and metamorphic ages vary systemically throughout the TNB, thereby supporting a model that includes D_2-related convergence and progressive tectonic thickening and regional metamorphism that lasted until at least ca. 1776 Ma.

Acknowledgments

This project would not have been possible without the support of the Manitoba Geological Survey, which provided field logistics and the thin sections. Thanks to Inco Limited (now Vale Limited) for providing access to their mine sites, and Crowflight Minerals Inc. (now CaNickel Mining Limited) for providing access to their diamond drillcore. Sincere thanks to J. Macek and H. Zwanzig for sharing their knowledge of the geology of the TNB, and to C. Böhm and T. Chacko for reading early drafts of this manuscript and providing advice for assessing the geochronological data. Thanks to two anonymous reviewers and editor R. Parrish for their constructive comments which served to improve the content of the manuscript. This research was partially supported by NSERC Discovery Grant 037233 to D. Pattison.

Appendix A. Supplementary data

Supplementary data associated with this article can be found, in the online version, at http://dx.doi.org/10.1016/j.precamres.2013.06.009.

References

Ansdell, K.M., 2005. Tectonic evolution of the Manitoba-Saskatchewan segment of the Paleoproterozoic Trans-Hudson Orogen, Canada. Canadian Journal of Earth Sciences 42, 741–759.

Bailes, A.H., Böhm, C.O., 2008. Detrital zircon provenance of the Saw Lake protoquartzite, east end of the exposed Flin Flon Domain, Manitoba. In: Manitoba Geological Survey, Report of Activities 2008., pp. 29–37.

Baxter, E.F., 2010. Diffusion of noble gases in minerals. In: Zhang, Y., Cherniak, D.J. (Eds.), Reviews in Mineralogy and Geochemistry, vol. 72, pp. 509–557.

Bell, C.K., 1971. History of the superior – Churchill boundary in Manitoba. In: Turnock, A.C. (Ed.), Geoscience Studies in Manitoba. Geological Association of Canada, pp. 5–10, Special Paper 9.

Bingen, B., van Breemen, O., 1998. U–Pb monazite ages in amphibolite- to granulite-facies orthogneiss reflect hydrous mineral breakdown reactions: Sveconorwegian Province of SW Norway. Contributions to Mineralogy and Petrology 132, 336–353.

Bleeker, W., 1990a. Evolution of the Thompson Nickel Belt and Its Nickel Deposits, Manitoba, Canada. University of New Brunswick, Fredericton, New Brunswick, Canada (Ph.D. Thesis).

Bleeker, W., 1990b. New structural–metamorphic constraints on Early Proterozoic oblique collision along the Thompson Nickel Belt, Manitoba, Canada. In: Lewry, J.F., Stauffer, M.R. (Eds.), The Early Proterozoic Trans-Hudson Orogen of North America. Geological Association of Canada, pp. 57–73, Special Paper 37.

Bleeker, W., Nägerl, P., Machado, N., 1995. The Thompson Nickel Belt, Manitoba: some new U–Pb ages. In: Geological Association of Canada – Mineralogical Association of Canada Joint Annual Meeting, Program with Abstracts 20, p. 8.
Bleeker, W., Macek, J., 1996. Evolution of the Thompson Nickel Belt, Manitoba: setting of Ni–Cu deposits in the western part of the circum Superior Boundary Zone. In: Geological Association of Canada – Mineralogical Association of Canada Joint Annual Meeting, Field Trip Guidebook A1, p. 45.
Bleeker, W., Hamilton, M.A., 2001. New SHRIMP U–Pb ages for the Ospwagan Group: implications for the SE margin of the Trans-Hudson Orogen. In: Geological Association of Canada – Mineralogical Association of Canada Joint Annual Meeting, Program with Abstracts 26, p. 15.
Burnham, O.M., Halden, N., Layton-Matthews, D., Lesher, C.M., Liwanag, J., Heaman, L., Hulbert, L., Machado, N., Michalak, D., Pacey, M., Peck, D.C., Potrel, A., Theyer, P., Toope, K., Zwanzig, H., 2009. CAMIRO Project 97E-02, Thompson Nickel Belt: final report March 2002, revised and updated 2003. Manitoba Geological Survey, Open File OF2008-11, CD-ROM.
Corrigan, D., Pehrsson, S., Wodicka, N., de Kemp, E., 2009. The Paleoproterozoic Trans-Hudson Orog: a prototype of modern accretionary processes. In: Murphy, J.B., Keppie, J.D., Hynes, A.J. (Eds.), Ancient Orogens and Modern Analogues. Geological Society of London, pp. 457–479, Special Publication 327.
Couëslan, C.G., 2012. The Grass River Project: geological mapping at Phillips Lake, and new geochronological results from Paint Lake and Manasan Falls, Thompson Nickel Belt, central Manitoba. In: Manitoba Geological Survey, Report of Activities 2012., pp. 68–78.
Couëslan, C.G., Pattison, D.R.M., Tinkham, D.K., 2011. Regional low-pressure amphibolite-facies metamorphism at the Pipe II Mine, Thompson Nickel Belt, Manitoba, and comparison of metamorphic isograds in metapelites and meta-iron formations. The Canadian Mineralogist 49, 721–747.
Couëslan, C.G., Pattison, D.R.M., 2012. Low-pressure regional amphibolite-facies to granulite-facies metamorphism of the Paleoproterozoic Thompson Nickel Belt, Manitoba. Canadian Journal of Earth Sciences 49, 1117–1153.
Ellis, S., Beaumont, C., 1999. Models for convergent boundary tectonics: implications for the interpretation of Lithoprobe data. Canadian Journal of Earth Sciences 36, 1711–1741.
Fleet, M.E., 2003. Micas, second ed. The Geological Society, Rock Forming Minerals 3A.
Foster, G., Parrish, R.R., 2003. Metamorphic monazite and the generation of P–T–t paths. In: Vance, D., Müller, W., Villa, I.M. (Eds.), Geochronology: Linking the Isotopic Record with Petrology and Textures. Geological Society of London, pp. 25–47, Special Publication 220.
Gapais, D., Potrel, A., Machado, N., Hallot, E., 2005. Kinematics of long-lasting Paleoproterozoic transpression within the Thompson Nickel Belt, Manitoba, Canada. Tectonics 24, 1–16, http://dx.doi.org/10.1029/2004TC001700.
Gasser, D., Bruand, E., Rubatto, D., Stüwe, K., 2012. The behavior of monazite from greenschist facies phyllites to anatectic gneisses: an example from the Chugach Metamorphic Complex, southern Alaska. Lithos 134–135, 108–122.
Harte, B., Pattison, D.R.M., Linklater, C., 1991. Field relations and petrography of partially melted pelitic and semipelitic rocks. In: Voll, G., Topel, J., Pattison, D.R.M., Seifert, F. (Eds.), Equilibrium and Kinetics in Contact Metamorphism: The Ballachulish Igneous Complex and its Thermal Aureole. Springer Verlag, Heidelberg, pp. 181–209.
Hartel, T.H.D., Pattison, D.R.M., 1996. Genesis of Kapuskasing (Ontario) migmatitic mafic granulites by dehydration melting of amphibolite: the importance of quartz to reaction progress. Journal of Metamorphic Geology 14, 591–611.
Heaman, L.M., Peck, D., Toope, K., 2009. Timing and geochemistry of 1.88 Ga Molson Igneous Events, Manitoba: insights into the formation of a craton-scale magmatic and metallogenic province. Precambrian Research 172, 143–162.
Heaman, L.M., Böhm, Ch.O., Machado, N., Krogh, T.E., Weber, W., Corkery, M.T., 2011. The Pikwitonei Granulite Domain, Manitoba: a giant Neoarchean high-grade terrane in the northwest Superior Province. Canadian Journal of Earth Sciences 48, 205–245.
Holland, T.J.B., Powell, R., 1998. An internally-consistent thermodynamic dataset for phases of petrological interest. Journal of Metamorphic Geology 16, 309–344.
Holness, M.B., Sawyer, E.W., 2008. On the pseudomorphing of melt-filled pores during the crystallization of migmatites. Journal of Petrology 49, 1343–1363.
Hoskin, P.W.O., Black, L.P., 2000. Metamorphic zircon formation by solid-state recrystallization of protolith igneous zircon. Journal of Metamorphic Geology 18, 423–439.
Hubregtse, J.J.M.W., 1980. The Archean Pikwitonei Granulite Domain and Its Position at the Margin of the Northwestern Superior Province (Central Manitoba). Manitoba Mineral Resources Division, Geological Paper GP80-3.
Hulbert, L., Stern, R., Kyser, T.K., Pearson, J., Lesher, M., Grinenko, L., 1994. The Winnipegosis komatiite belt central Manitoba. In: Manitoba Energy and Mines, Manitoba Mining, Minerals, and Petroleum Convention 1994, Program, p. 21.
Hulbert, L.J., Hamilton, M.A., Horan, M.F., Scoates, R.F.J., 2005. U–Pb zircon and Re–Os isotope geochronology of mineralized ultramafic intrusions and associated nickel ores from the Thompson Nickel Belt, Manitoba, Canada. Economic Geology 100, 29–41.
Janots, E., Brunet, F., Goffé, B., Poinssot, C., Burchard, M., Cemič, L., 2007. Thermochemistry of monazite-(La) and dissakisite-(La): implications for monazite and allanite stability in metapelites. Contributions to Mineralogy and Petrology 154, 1–14.
Janots, E., Engi, M., Berger, A., Allaz, J., Schwarz, J.-O., Spandler, C., 2008. Prograde metamorphic sequence of REE minerals in pelitic rocks of the Central Alps: implications for allanite–monazite–xenotime phase relations from 250 to 610 °C. Journal of Metamorphic Geology 26, 509–526.
Kelly, N.M., Clarke, G.L., Harley, S.L., 2006. Monazite behaviour and age significance in poly-metamorphic high-grade terrains: a case study from the western Musgrave Block, central Australia. Lithos 88, 100–134.
Kelsey, D.E., Clark, C., Hand, M., 2008. Thermobarometric modelling of zircon and monazite growth in melt-bearing systems: examples using model metapelitic and metapsammitic granulites. Journal of Metamorphic Geology 26, 199–212.
Kingsbury, J.A., Miller, C.F., Wooden, J.L., Harrison, T.M., 1993. Monazite petrogenesis and U–Pb systematics in rocks of the eastern Mojave Desert, California, USA: implications for thermochronology. Chemical Geology 110, 147–167.
Kretz, R., 1983. Symbols for rock-forming minerals. American Mineralogist 68, 277–279.
Kuiper, Y.D., Lin, S., Böhm, C.O., 2011. Himalayan-type escape tectonics along the Superior Boundary Zone in Manitoba, Canada. Precambrian Research 187, 248–262.
Lewry, J.F., Thomas, D.J., Macdonald, R., Chiarenzelli, J., 1990. Structural relations in accreted terranes of the Trans-Hudson Orogen, Saskatchewan: telescoping in a collisional regime? In: Lewry, J.F., Stauffer, M.R. (Eds.), The Early Proterozoic Trans-Hudson Orogen of North America. Geological Association of Canada, pp. 75–94, Special Paper 37.
Ludwig, K.R., 2003. Isoplot 3.00: a geochronological toolkit for Microsoft Excel. Berkeley Geochronology Center, Special Publication 4.
Machado, N., Krogh, T.E., Weber, W., 1990. U–Pb geochronology of basement gneisses in the Thompson Belt (Manitoba): evidence for pre-Kenoran and Pikwitonei-type crust and Early Proterozoic basement reactivation in the western margin of the Archean Superior Province. Canadian Journal of Earth Sciences 27, 794–802.
Machado, N., Gapais, D., Potrel, A., Gauthier, G., Hallot, E., 2011a. Chronology of transpression, magmatism, and sedimentation in the Thompson Nickel Belt (Manitoba, Canada) and timing of Trans-Hudson Orogen – Superior Province collision. Canadian Journal of Earth Sciences 48, 295–324.
Machado, N., Heaman, L.M., Krogh, T.E., Weber, W., Corkery, T.M., 2011b. Timing of Paleoproterozoic granitoid magmatism along the northwestern Superior Province margin: implications for the tectonic evolution of the Thompson Nickel Belt. Canadian Journal of Earth Sciences 48, 325–346.
Mezger, K., Bohlen, S.R., Hanson, G.N., 1990. Metamorphic history of the Archean Pikwitonei Granulite Domain and the Cross Lake Subprovince, Superior Province, Manitoba, Canada. Journal of Petrology 31, 483–517.
Montel, J-.M., 1993. A model for monazite/melt equilibrium and application to the generation of granitic magmas. Chemical Geology 110, 127–146.
Pattison, D.R.M., 1992. Stability of andalusite and sillimanite and the Al_2SiO_5 triple point: constraints from the Ballachulish aureole, Scotland. Journal of Geology 100, 423–446.
Percival, J.A., Whalen, J.B., Rayner, N., 2004. Pikwitonei–Snow Lake, Manitoba transect, Trans-Hudson Orogen–Superior Margin Metallotect Project: initial geological, isotopic, and SHRIMP U–Pb results. In: Manitoba Geological Survey, Report of Activities 2004., pp. 120–134.
Percival, J.A., Whalen, J.B., Rayner, N., 2005. Pikwitonei–Snow Lake, Manitoba transect, Trans-Hudson Orogen–Superior Margin Metallotect Project: new results and tectonic interpretation. In: Manitoba Geological Survey, Report of Activities 2005., pp. 69–91.
Percival, J.A., Zwanzig, H.V., Rayner, N., 2006. New tectonostratigraphic framework for the northeastern Kisseynew Domain, Manitoba. In: Manitoba Geological Survey, Report of Activities 2006., pp. 74–84.
Pyle, J.M., Spear, F.S., 2003. Four generations of accessory-phase growth in low-pressure migmatites from SW New Hampshire. American Mineralogist 88, 338–351.
Rapp, R.P., Watson, E.B., 1986. Monazite solubility and dissolution kinetics: implications for the thorium and light rare earth chemistry of felsic magmas. Contributions to Mineralogy and Petrology 94, 304–316.
Rapp, R.P., Ryerson, F.J., Miller, C.F., 1987. Experimental evidence bearing on the stability of monazite during crustal anatexis. Geophysical Research Letters 14, 307–310.
Rasmussen, B., Muhling, J.R., Fletcher, I.R., Wingate, M.T.D., 2006. In situ SHRIMP U–Pb dating of monazite integrated with petrology and textures: does bulk composition control whether monazite forms in low-Ca pelitic rocks during amphibolite facies metamorphism? Geochimica et Cosmochimica Acta 70, 3040–3058.
Rayner, N., Zwanzig, H.V., Percival, J.A., 2006. Detrital zircon provenance of the Pipe Formation, Ospwagan Group, Thompson Nickel Belt, Manitoba. In: Manitoba Geological Survey, Report of Activities 2006., pp. 116–124.
Sawyer, E.W., 1999. Criteria for the recognition of partial melting. Physics and Chemistry of the Earth (Part A) 24, 269–279.
Schaltegger, U., Fanning, C.M., Günther, D., Maurin, J.C., Schulmann, K., Gebauer, D., 1999. Growth, annealing and recrystallization of zircon and preservation of monazite in high-grade metamorphism: conventional and in situ U–Pb isotope, cathodoluminescence and microchemical evidence. Contributions to Mineralogy and Petrology 134, 186–201.
Schneider, D.A., Heizler, M.T., Bickford, M.E., Wortman, G.L., Condie, K.C., Perilli, S., 2007. Timing constraints of orogeny to cratonization: thermochronology of the Paleoproterozoic Trans-Hudson Orogen, Manitoba and Saskatchewan, Canada. Precambrian Research 153, 65–95.
Scoates, J.S., Wall, C.J., Friedman, R.M., Booth, K., Scoates, R.F.J., Couëslan, C., Macek, J., 2010. Recent progress in determining the precise age of ultramafic sills and mafic dikes associated with mineralization in the Thompson Nickel Belt,

Manitoba, Canada. In: Brown, G.H., Jugo, P.J., Lesher, C.M., Mungall, J.E. (Eds.), 11th International Platinum Symposium. 21–24 June 2010, Sudbury, Ontario, Canada, Abstracts. Ontario Geological Survey, Miscellaneous Release – Data 269.

Scoates, R.F.J., Macek, J.J., Russell, J.K., 1977. Thompson Nickel Belt Project. In: Manitoba Mineral Resources Division, Report of Field Activities 1977., pp. 47–53.

Shore, M., Fowler, A.D., 1996. Oscillatory zoning in minerals: a common phenomenon. The Canadian Mineralogist 34, 1111–1126.

Simonetti, A., Heaman, L.M., Hartlaub, R.P., Creaser, R.A., MacHattie, T.G., Böhm, C., 2005. U–Pb zircon dating by laser ablation–MC–ICP–MS using a new multiple ion counting Faraday collector array. Journal of Analytical Atomic Spectrometry 20, 677–686.

Simonetti, A., Heaman, L.M., Chacko, T., Banerjee, N.R., 2006. In situ petrographic thin section U–Pb dating of zircon, monazite, and titanite using laser ablation–MC–ICP–MS. International Journal of Mass Spectrometry 253, 87–97.

Spear, F.S., 1993. Metamorphic Phase Equilibria and Pressure–Temperature–Time Paths. Mineralogical Society of America, Washington, D.C.

Spear, F.S., 2010. Monazite-allanite phase relations in metapelites. Chemical Geology 279, 55–62.

Spear, F.S., Pyle, J.M., 2010. Theoretical modelling of monazite growth in a low-Ca metapelite. Chemical Geology 273, 111–119.

Stauffer, M.R., 1984. Manikewan: an Early Proterozoic ocean in central Canada, its igneous history and orogenic closure. Precambrian Research 25, 257–281.

Tomkins, H.S., Pattison, D.R.M., 2007. Accessory phase petrogenesis in relation to major phase assemblages in pelites from the Nelson contact aureole, southern British Columbia. Journal of Metamorphic Petrology 25, 401–421.

White, D.J., Lucas, S.B., Hajnal, Z., Green, A.G., Lewry, J.F., Weber, W., Bailes, A.H., Syme, E.C., Ashton, K., 1994. Paleoproterozoic thick-skinned tectonics: lithoprobe seismic reflection results from the eastern Trans-Hudson Orogen. Canadian Journal of Earth Sciences 31, 458–469.

White, D.J., Jones, A.G., Lucas, S.B., 1999. Tectonic evolution of the Superior Boundary Zone from coincident seismic reflection and magnetotelluric profiles. Tectonics 18, 430–451.

White, D.J., Lucas, S.B., Bleeker, W., Hajnal, Z., Lewry, J.F., Zwanzig, H.V., 2002. Suture-zone geometry along an irregular Paleoproterozoic margin: the Superior boundary zone, Manitoba, Canada. Geology 30, 735–738.

Williams, M.L., Jercinovic, M.J., 2002. Microprobe monazite geochronology: putting absolute time into microstructural analysis. Journal of Structural Geology 24, 1013–1028.

Wing, B.A., Ferry, J.M., Harrison, T.M., 2003. Prograde destruction and formation of monazite and allanite during contact and regional metamorphism of pelites: petrology and geochronology. Contributions to Mineralogy and Petrology 145, 228–250.

Wolf, M.B., London, D., 1995. Incongruent dissolution of REE- and Sr-rich apatite in peraluminous granitic liquids: differential apatite, monazite, and xenotime solubilities during anatexis. American Mineralogist 80, 765–775.

Yang, P., Pattison, D., 2006. Genesis of monazite and Y zoning in garnet from the Black Hills, South Dakota. Lithos 88, 233–253.

Yardley, B.W.D., 1989. An Introduction to Metamorphic Petrology. Pearson Education Limited, Harlow, England.

Zwanzig, H.V., 1998. Structural mapping of the Setting Lake area. In: Manitoba Geological Survey, Report of Activities 1998., pp. 40–45.

Zwanzig, H.V., Böhm, Ch.O., 2002. Tectonostratigraphy, Sm–Nd isotope and U–Pb age data of the Thompson Nickel Belt and Kisseynew north and east margins, Manitoba. In: Manitoba Geological Survey, Report of Activities 2002., pp. 102–114.

Zwanzig, H.V., Böhm, C.O., Potrel, A., Machado, N., 2003. Field relations, U–Pb zircon ages and Nd model ages of granitoid intrusions along the Thompson Nickel Belt–Kisseynew Domain boundary, Setting Lake area. In: Manitoba Geological Survey, Report of Activities 2003., pp. 118–129.

Zwanzig, H.V., Murphy, L., Percival, J.A., Whalen, J.B., Rayner, N., 2006. Thompson Nickel Belt–type units in the northeastern Kisseynew Domain, Manitoba. In: Manitoba Geological Survey, Report of Activities 2006., pp. 85–103.

Zwanzig, H.V., Macek, J.J., McGregor, C.R., 2007. Lithostratigraphy and geochemistry of the high-grade metasedimentary rocks in the Thompson Nickel Belt and adjacent Kisseynew Domain, Manitoba: implications for nickel exploration. Economic Geology 102, 1197–1216.

Zwanzig, H.V., Bailes, A.H., 2010. Geology and geochemical evolution of the northern Flin Flon and southern Kisseynew domains, Kississing–File lakes area, Manitoba. In: Manitoba Geological Survey, Geoscientific Report GR2010-1.